

Supplementary Information for Regions of Interest as nodes of dynamic functional brain networks

Elisa Ryypö¹, Enrico Glerean^{2,3}, Elvira Brattico⁴, Jari Saramäki¹, and Onerva Korhonen^{1,2,*}

¹Department of Computer Science, School of Science, Aalto University, Espoo, Finland

²Turku PET Centre, University of Turku, Turku, Finland

³Department of Neuroscience and Biomedical Engineering, School of Science, Aalto University, Espoo, Finland

⁴Center for Music in the Brain, Department of Clinical Medicine, Aarhus University, & The Royal Academy of Music Aarhus/Aalborg, Denmark

*Corresponding author: Onerva Korhonen, email:
onerva.korhonen@aalto.fi

1 Supplementary methods

1.1 Selection of time window length

For constructing time-dependent functional networks from fMRI data, we needed to divide the measurement time series into time windows. We used sliding windows that were 80 samples (160s) long; overlap between two consecutive windows was 50%. Selecting the length of the time window required compromising. On the one hand, we wanted to have as many time windows as possible in order to maximize the number of data points in the analysis of temporal variation in spatial consistency. On the other hand, we wanted to avoid possible distortion in Pearson correlation coefficient and, consecutively, in spatial consistency caused by too short time windows.

To find the optimal window length, we placed a time window at the beginning of the measurement time series. The length of this time window varied between $l = 5$ and $l = 195$ samples with steps of 5 samples. Length of the last time window was comparable to the length of the entire time series (244 samples). In each of the time windows, we calculated

spatial consistency of each ROI. Then, we investigated the mean spatial consistency over ROIs. These calculations were done separately for each subject of both the in-house dataset and the ABIDE dataset.

Behaviour of the mean spatial consistency as a function of the window length was similar for most subjects. First, spatial consistency increased with the window length, showing that short window lengths may have distorted values of spatial consistency. For some subjects, the increase of spatial consistency was followed by a rapid decrease. At larger window lengths, spatial consistency of all subjects saturated and stayed stable when the window length approached the length of the entire time series. The window length used in the present study, 80 samples, was for all subjects located in the saturation area; for some subjects it was in the beginning of the saturation, whereas for others the saturation had happened already at shorter window lengths.

The variation in the exact beginning point of the saturation area seems to suggest that for different subjects, different window lengths could be used. However, changing the window length does not affect the mean spatial consistency as long as the selected window length stays in the saturation area. In particular, decreasing the window length within the saturation area does not improve the accuracy of correlation-based measures. In the present study we do group-level analysis by averaging values of spatial and spatiotemporal consistency as well as network turnover across subjects. Therefore, it is reasonable to use the same window length for all subjects to ensure that the consistency values of all subjects are obtained from the same amount of data.

It has been suggested that when studying dynamic functional connectivity, the time window length should be equal to or larger than $1/f_{min}$, where f_{min} is the lowest signal frequency present in the data (Leonardi & Van De Ville, 2015; Shakil, Billings, Keilholz, & Lee, 2017; Shakil, Keilholz, & Lee, 2015). In our preprocessing pipeline, the data are temporally filtered so that the lowest frequency remaining in the data is 0.01 Hz. The minimum time window length corresponding to this f_{min} is 100s or 50 samples which is smaller than the selected length of 80 samples. Similar lengths of time windows have been used in the literature (Bassett et al., 2011, 2013).

We performed the above-described window length optimization using both non-overlapping windows and sliding windows with 50% overlap. Since at window length of 80 samples there was no visible difference in mean spatial consistency between these two window types, we decided to use sliding windows to maximize the overall number of windows.

Time windows do not capture fluctuations slower than $1/l_{window}$, where l_{window} is the window length. If these fluctuations co-vary with spatial consistency, they may affect the obtained behavior of spatial consistency as a function of window length. In particular, these effects may be present at short window lengths, in which case additional high-pass filtering could change the behavior of spatial consistency as a function of window length and possibly lead to earlier saturation. However, at the selected window length, these fluctuations should be slower than $1/160s = 0.00625\text{Hz}$. This is slower than the lower bound of the band-pass filter applied in the preprocessing. Therefore, it is safe to assume that the selected window length, 80 samples, would be located in the saturation area also in

high-pass filtered data and that additional high-pass filtering would not change the results obtained with this window length.

1.2 Selection of the closest neighborhood size

Network turnover quantifies the tendency of ROI's closest neighborhood to change in time. The closest neighborhood is defined as a set of neighbors most strongly connected to the ROI. To determine an optimal size for the closest neighborhood, we calculated for all subjects of the in-house dataset the mean Jaccard index over time window pairs using a set of closest neighborhood sizes ranging from 5 to 195 with steps of 5. For each ROI, we averaged the Jaccard indices over subjects.

On average, the Jaccard index increased with the increasing closest neighborhood size. However, behavior of all ROIs was not similar. For some ROIs, the Jaccard index increased with the increasing closest neighborhood size over all neighborhood sizes. For other ROIs, however, the Jaccard index decreased with the increasing closest neighborhood size when the neighborhood size was small and started to increase only later. At larger neighborhood sizes, the behavior of the Jaccard index was same for all ROIs. The closest neighborhood size used in the present study, 35, was selected from the area where the differences between ROIs disappear and the Jaccard index begins to increase monotonically.

Investigating turnover in the closest neighborhoods is effectively close to thresholding the network and therefore may exclude from the analysis some functionally meaningful connections. This could be avoided by quantifying the changes in network structure in terms of some similarity measure that does not require thresholding. In this case, a connectivity profile of each ROI would be defined as a vector containing the Pearson correlation coefficients between the time series of the ROI and all other ROIs. Then, for example Spearman rank correlation or Kendall's Tau could be used to quantify the similarity of connectivity profiles obtained in consecutive time windows. The difference between Jaccard index calculated in the closest neighborhoods and the non-thresholding methods is not big: in data pooled across ROIs and subjects, the Pearson correlation coefficient between the Jaccard index and Spearman rank correlation was $r = 0.78$, between the Jaccard index and Kendall's tau $r = 0.80$, and between Spearman rank correlation and Kendall's tau $r = 0.99$.

Although the connectivity profiles are guaranteed to include all significant connections, they contain also a remarkable amount of weak correlations that are caused by rather random similarities in time series. Since these correlations do not reflect any actual functional connection, one may expect their strength to change randomly between consecutive time windows. To avoid this noise in the network structure, we decided to accept the possible drawbacks of thresholding and investigate the closest neighborhoods of 35 neighbors.

1.3 ABIDE data

In order to investigate how our results generalize for other datasets, we repeated all analyses for a secondary, independent dataset. This dataset was collected as a part of the Autism Brain Imaging Data Exchange (ABIDE) initiative ([Di Martino et al., 2014](#)). We refer to this dataset as the ABIDE data.

Subjects

The ABIDE dataset included resting-state data of 31 healthy subjects that were measured at NYU Langone Medical Center. During the preprocessing and quality control, 3 of these subjects were excluded due to exceptional amount of motion. This left for further analysis 28 subjects (7 female, 21 male, age 29.9 ± 3.8 , mean \pm SD). Based on Structured Clinical Interview for DSM-IV-TR Axis-I Disorders, Non-patient Edition (SCID-I/NP) and Adult ADHD Clinical Diagnostic Scale (ACDS) questionnaires, the subjects did not suffer from autism spectrum disorders. The ABIDE IDs of the subjects were 51057, 51058, 51059, 51060, 51061, 51062, 51063, 51066, 51067, 51112, 51113, 51114, 51115, 51116, 51117, 51118, 51119, 51130, 51131, 51146, 51147, 51148, 51149, 51151, 51152, 51153, 51154, and 51155.

Data acquisition

Subjects were measured with a 3T Allegra MRI device (Siemens Medical Solutions, NJ, USA). Structural MR images were acquired with a T1-weighted MP-RAGE sequence with voxel size of $1.3 \times 1.0 \times 1.3$ mm 3 . Resting-state fMRI data were measured as a T2*-weighted EPI-sequence with the following parameters: TR = 2.0s, TE = 15ms, flip angle = 90° , voxel size = $3.0 \times 3.0 \times 5$ mm 3 , matrix size = $80 \times 80 \times 33$, FOV = 240×240 mm 2 . The length of the data was 6 minutes (180 time points). During the measurement, subjects were instructed to relax with their eyes open, while a white cross-hair against a black background was projected on a screen. However, some subjects may have closed their eyes regardless of instructions.

Preprocessing and analyses

The ABIDE dataset went through the same preprocessing and analyses as the in-house dataset (see the main text for details).

We analysed the ABIDE dataset using 245 ROIs from the Brainnetome atlas. The size of these ROIs, measured as the number of voxels, varied between 8 and 1148 with mean being 362.7, SD being 235.9, and median being 299. Note that location of one ROI, right thalamus (8_8) did not overlap over all subjects of the ABIDE dataset, and this ROI was therefore excluded from the analysis.

2 Supplementary results

2.1 In-house data analysed with AAL, HO, and Craddock 200/400 atlases

For investigating the time-dependent behavior of functional homogeneity and changes in local network structure in our in-house dataset, we used five different parcellations of the brain: the connectivity-based Brainnetome atlas and Craddock 200/400 parcellations as well as anatomical Automated Anatomical Labeling (AAL) and HarvardOxford (HO) atlases. In the main article, we have reported the results obtained using Brainnetome. The results obtained with the Craddock parcellations, AAL, and HO were very similar. For detailed discussion of the results, the reader is referred to the Results section of the main article.

Functional homogeneity, measured in terms of static spatial consistency, varies a lot between ROIs of Brainnetome, Craddock 200/400, AAL, and HO, as we have reported in the main article (see Fig. 1 of the main article). For investigating the time-dependent behavior of spatial consistency, we divided the data into five time windows. There is no visible difference between distributions of spatial consistency calculated in different time windows for either AAL, HO, or the Craddock parcellations (Fig. S1). In both AAL and HO, static spatial consistency is negatively correlated with ROI size (AAL: $r = -0.32$, $p = 4.13 \times 10^{-4}$; HO: $r = -0.33$, $p = 8.62 \times 10^{-5}$; Fig. S10A, D). In the Craddock parcellations, there is no significant correlation between static spatial consistency and ROI size (Craddock 200: $r = -8.31 \times 10^{-4}$, $p = 0.991$; Craddock 400: $r = 0.031$, $p = 0.538$; Fig. S11A, D).

Although the pooled distributions of spatial consistency do not differ between time windows, there are significant relative changes in the spatial consistency of single ROIs (Fig. S2A, Fig. S3A, Fig. S4A, Fig. S5A). This leads to a nonuniform spatial distribution of spatiotemporal consistency that quantifies the changes in spatial consistency (Fig. S2B, Fig. S3B, Fig. S4B, Fig. S5B). The AAL and HO ROIs with the highest and lowest spatiotemporal consistency are listed in the main article. In the Craddock 200/400 parcellations, the ROI boundaries do not respect anatomical landmarks and ROIs are referred to by numbers instead of anatomical names. For the location of the Craddock ROIs with the highest spatiotemporal consistency, the reader is referred to Figs. S18 and S19. There is no significant correlation between ROI size and spatiotemporal consistency in either AAL, HO, or Craddock 200/400 parcellations (AAL: $r = 0.16$, $p = 0.0963$; HO: $r = -0.025$, $p = 0.770$; Craddock 200: $r = 0.028$, $p = 0.698$, Craddock 400: $r = 0.014$, $p = 0.780$; Fig. S10B, E and Fig. S11B, E).

Changes in the local network structure around AAL, HO, and Craddock 200/400 ROIs are visible as significant neighborhood turnover between subsequent time windows (Fig. S6A, Fig. S7A, Fig. S8A, Fig. S9A). This turnover is anatomically nonuniformly distributed and shows strong spatial correlation (Fig. S6B, Fig. S7B, Fig. S8B, Fig. S9B). The AAL and HO ROIs with the highest and lowest values of network turnover are listed in the main article; for the Craddock 200/400 ROIs with the highest and lowest network

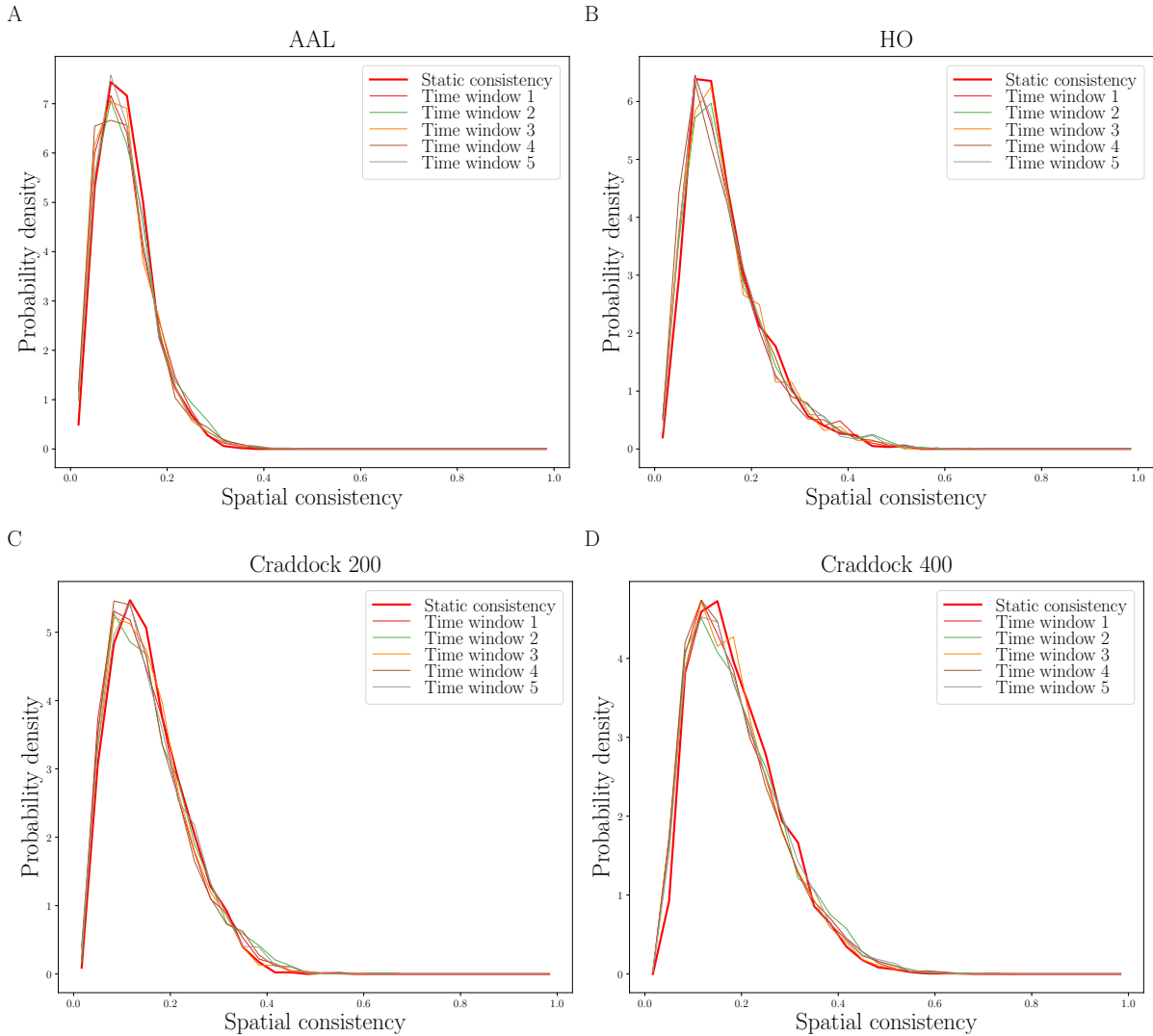


Figure S1: Distributions of spatial consistency calculated separately for five time windows of 80 samples for A) AAL, B) HO, C) Craddock 200, and D) Craddock 400 ROIs. There is no visible difference between the distributions calculated for different time windows. All distributions have been calculated from pooled data of 13 subjects.

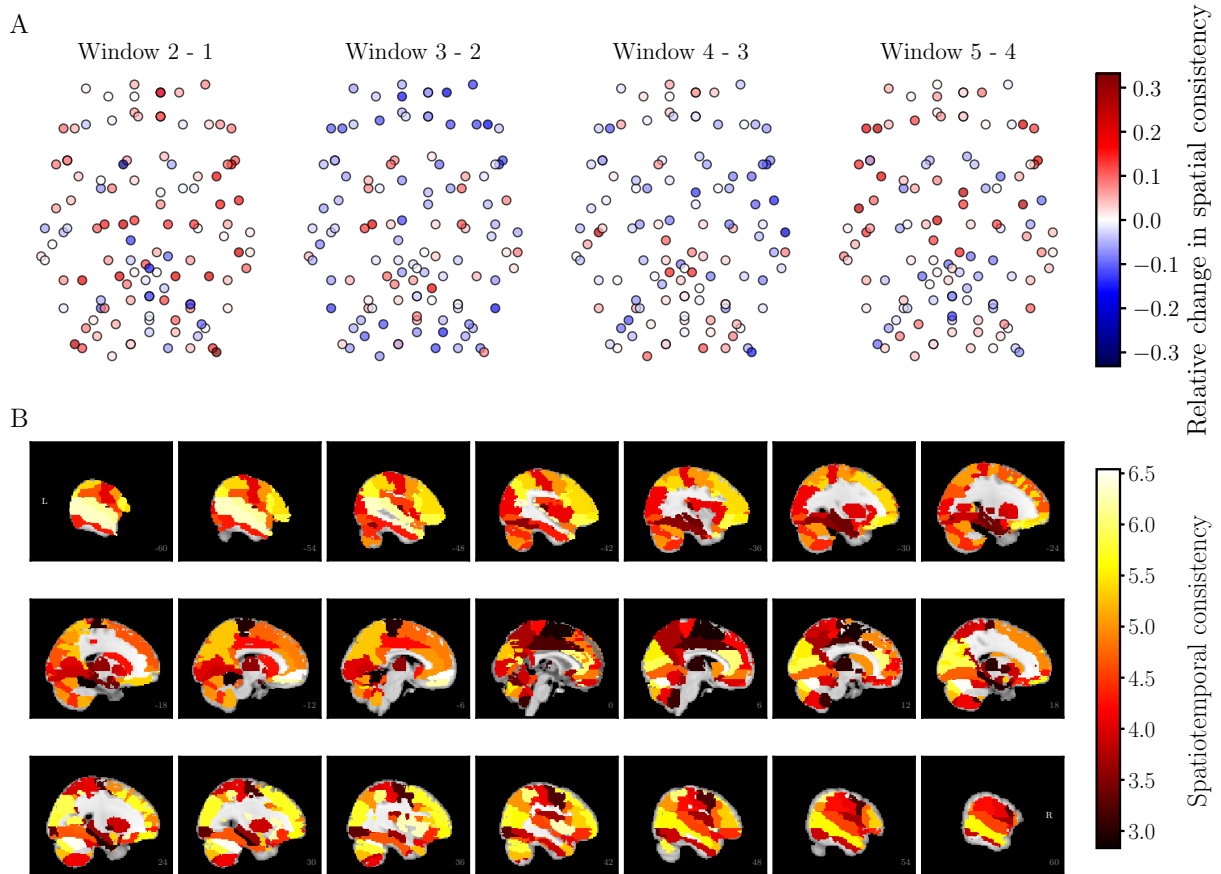


Figure S2: Spatial consistency changes in time. A) Relative changes in spatial consistency between subsequent time windows in the AAL atlas. The changes are non-randomly distributed in time and show strong spatial correlation, similarly as in the Brainnetome atlas (see Fig. 2 of the main article). The location of nodes is determined by a two-dimensional projection of the anatomical coordinates of ROI centroids similarly as in Fig. 2 of the main article. The visualization follows the neurological convention. B) The spatiotemporal consistency of AAL ROIs on brain surface. Spatiotemporal consistency has a non-uniform anatomical distribution and shows strong spatial correlation. All results are averaged over 13 subjects. Grayscale areas are not included in the present study (white matter).

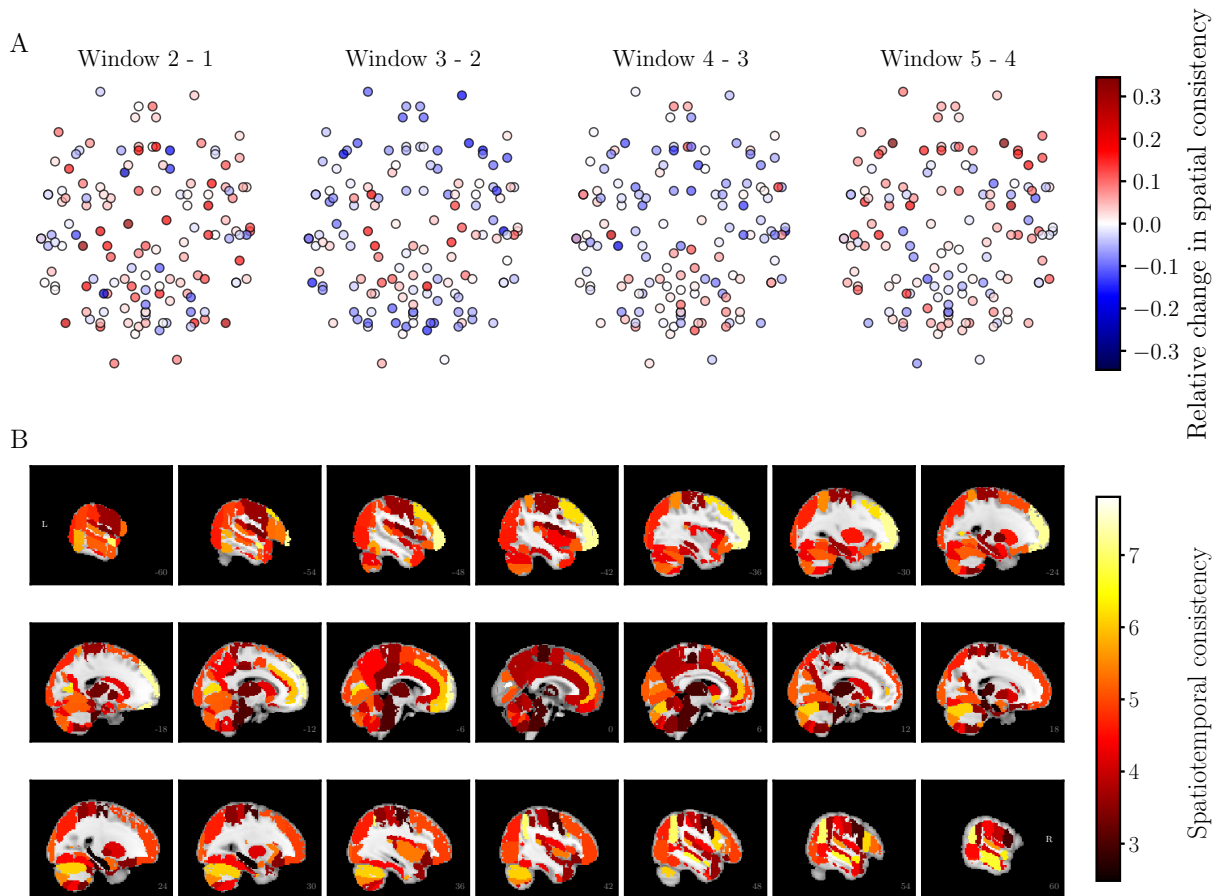


Figure S3: Time-dependent behavior of spatial consistency in HO atlas. A) Relative changes in spatial consistency between subsequent time windows. B) Spatiotemporal consistency on brain surface. All results are averaged over 13 subjects. For further details, see Fig. S2 and Fig. 2 of the main article.

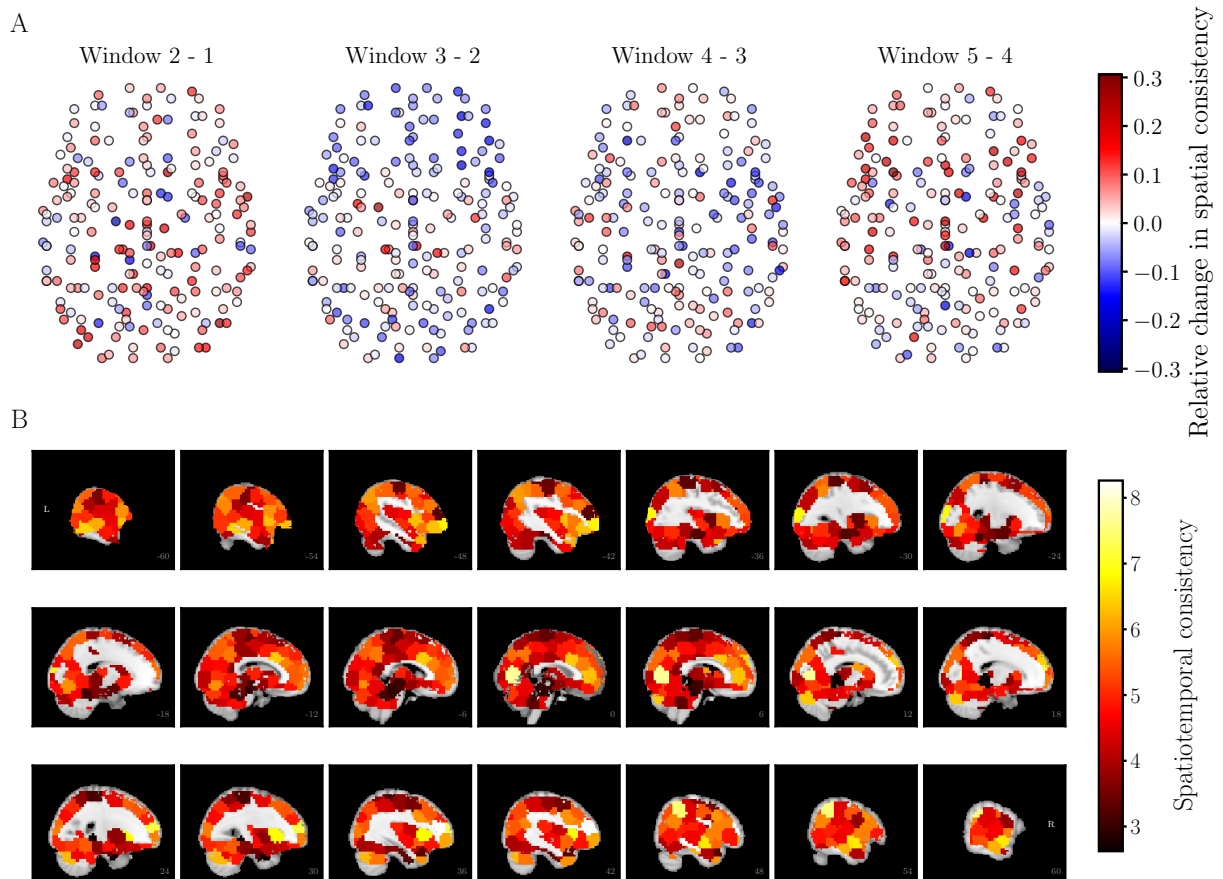


Figure S4: Time-dependent behavior of spatial consistency in the Craddock 200 atlas. A) Relative changes in spatial consistency between subsequent time windows. B) Spatiotemporal consistency on brain surface. All results are averaged over 13 subjects. For further details, see Fig. S2 and Fig. 2 of the main article.

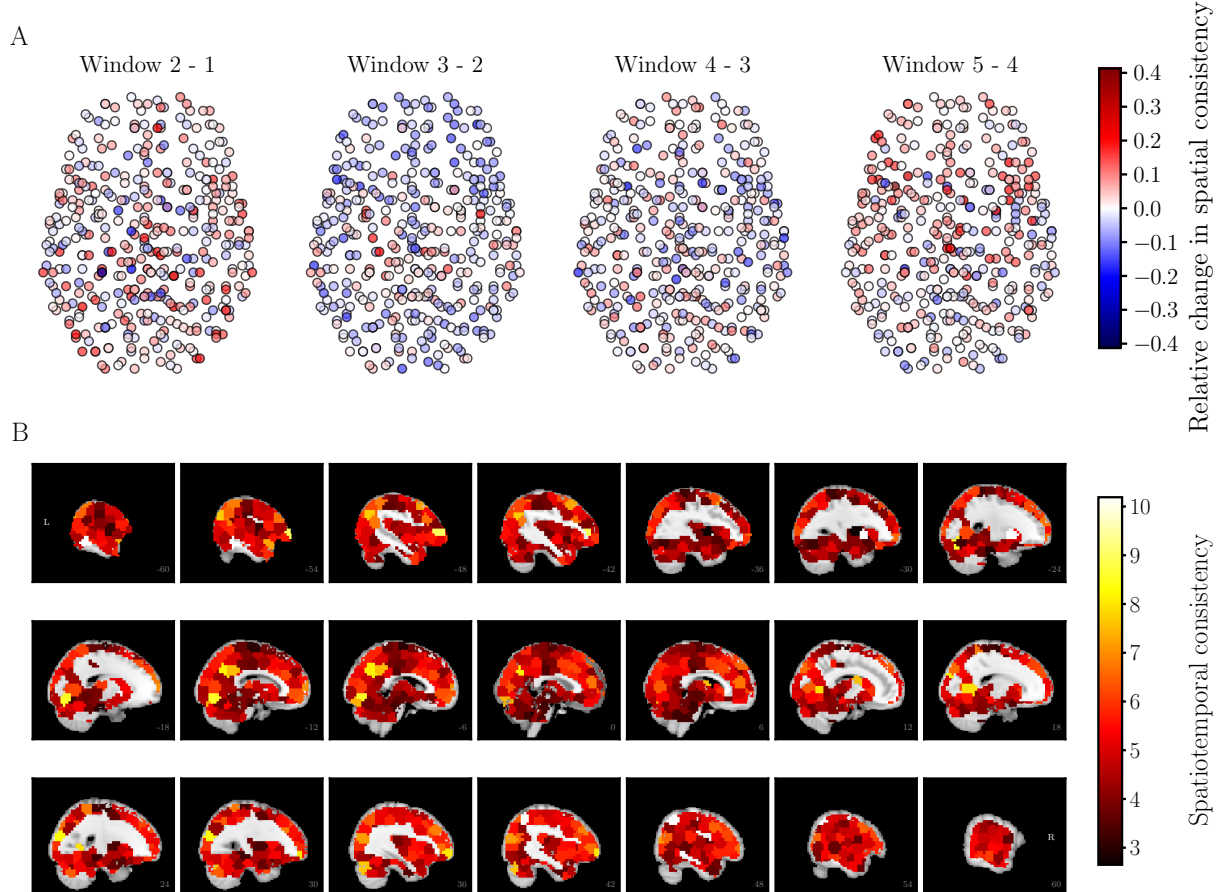


Figure S5: Time-dependent behavior of spatial consistency in the Craddock 400 atlas. A) Relative changes in spatial consistency between subsequent time windows. B) Spatiotemporal consistency on brain surface. All results are averaged over 13 subjects. For further details, see Fig. S2 and Fig. 2 of the main article.

turnover, the reader is referred to Fig. S18 and Fig. S19. In particular, subcortical and cerebellar areas tend to have high network turnover. Network turnover is negatively correlated with ROI size in AAL, HO, and Craddock 200/400 (AAL: $r = -0.42$, $p \ll 10^{-5}$; HO: $r = -0.30$, $p = 4.02 \times 10^{-4}$; Craddock 200: $r = -0.21$, $p = 0.00232$; Craddock 400: $r = -0.41$, $p \ll 10^{-5}$; Fig. S10C, F, Fig. S11C, F).

Spatiotemporal consistency and network turnover are negatively correlated in AAL, HO, and Craddock 200/400 similarly as in Brainnetome (AAL: $r = -0.38$, $p = 2.08 \times 10^{-5}$; HO: $r = -0.44$, $p \ll 10^{-5}$; Craddock 200: $r = -0.46$, $p \ll 10^{-5}$; Craddock 400: $r = -0.42$, $p \ll 10^{-5}$; Fig. S12A, Fig. S13A, Fig. S14A, Fig. S15A). ROIs with high static spatial consistency tend to have high spatiotemporal consistency and low network turnover in both AAL and HO as well as in both Craddock parcellations (Fig. S12B, Fig. S13B, Fig. S14B, Fig. S15B). In AAL, ROIs with high spatiotemporal consistency and low network turnover tend to be larger than ROIs with low spatiotemporal consistency and high network turnover, although the connection is not as clear as for Brainnetome ROIs (Fig. S12C). In HO or Craddock 200/400, such connection is not visible (Fig. S13C, Fig. S14C, Fig. S15C). Bearing in mind the lack of correlation between ROI size and spatiotemporal consistency in HO and Craddock 200/400 ROIs, as well as the spatiotemporal consistency and the relatively weak correlation between ROI size and network turnover in HO and Craddock 200, this result should not be surprising.

We used principal component analysis (PCA) to find two groups of extreme ROIs: five ROIs with high spatiotemporal consistency and low network turnover and five ROIs with low spatiotemporal consistency and high network turnover (Fig. S16, Fig. S17, Fig. S18, Fig. S19). In all parcellations, ROIs of the first extreme group are located in the cortex, whereas the second extreme group contains subcortical and cerebellar areas. For further methodological details, the reader is referred to the main article.

From each of the parcellations, we selected four extreme ROIs for further investigation. The selected AAL ROIs were orbital part of left middle frontal gyrus, right superior occipital gyrus, right olfactory cortex, and right globus pallidus. From HO, we selected left and right supracalcarine cortex, left globus pallidus, and right hippocampus. From Craddock 200, we selected for further analysis ROIs 25, 7, 198, and 68. The ROIs selected from Craddock 400 were ROIs 183, 207, 399, and 42. To investigate the internal connectivity of these ROIs, we calculated the voxel-level intra-ROI correlation matrices (Fig. S20, Fig. S21). Rich, time-dependent connectivity structure is visible in all these ROIs, similarly as in Brainnetome ROIs. Although the overall voxel-level correlation is higher in ROIs with high spatiotemporal consistency, the correlations are not uniformly distributed. Instead, voxels are divided into several internally highly correlated subareas in all investigated ROIs. The time-dependent changes in the internal connectivity structure do not depend on the spatiotemporal consistency neither.

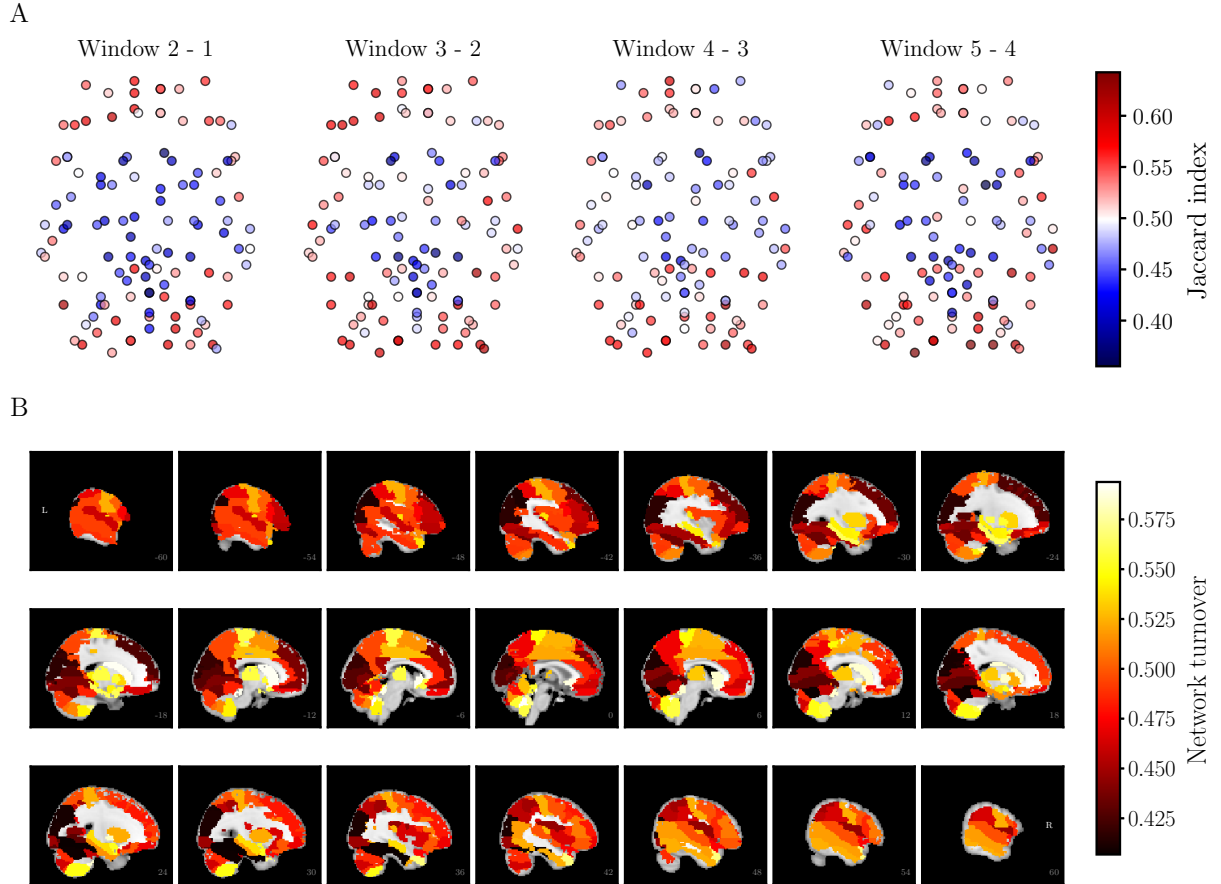


Figure S6: Strong neighborhood turnover takes place in dynamic functional brain networks. A) The Jaccard index between subsequent time windows in the AAL atlas. Values of the Jaccard index are spatially nonuniformly distributed and show strong spatial correlation, similarly as in the Brainnetome atlas (see Fig. 3 of the main article). Node locations are as in Fig. S2. B) Network turnover of AAL ROIs on brain surface. All results are averaged over 13 subjects.

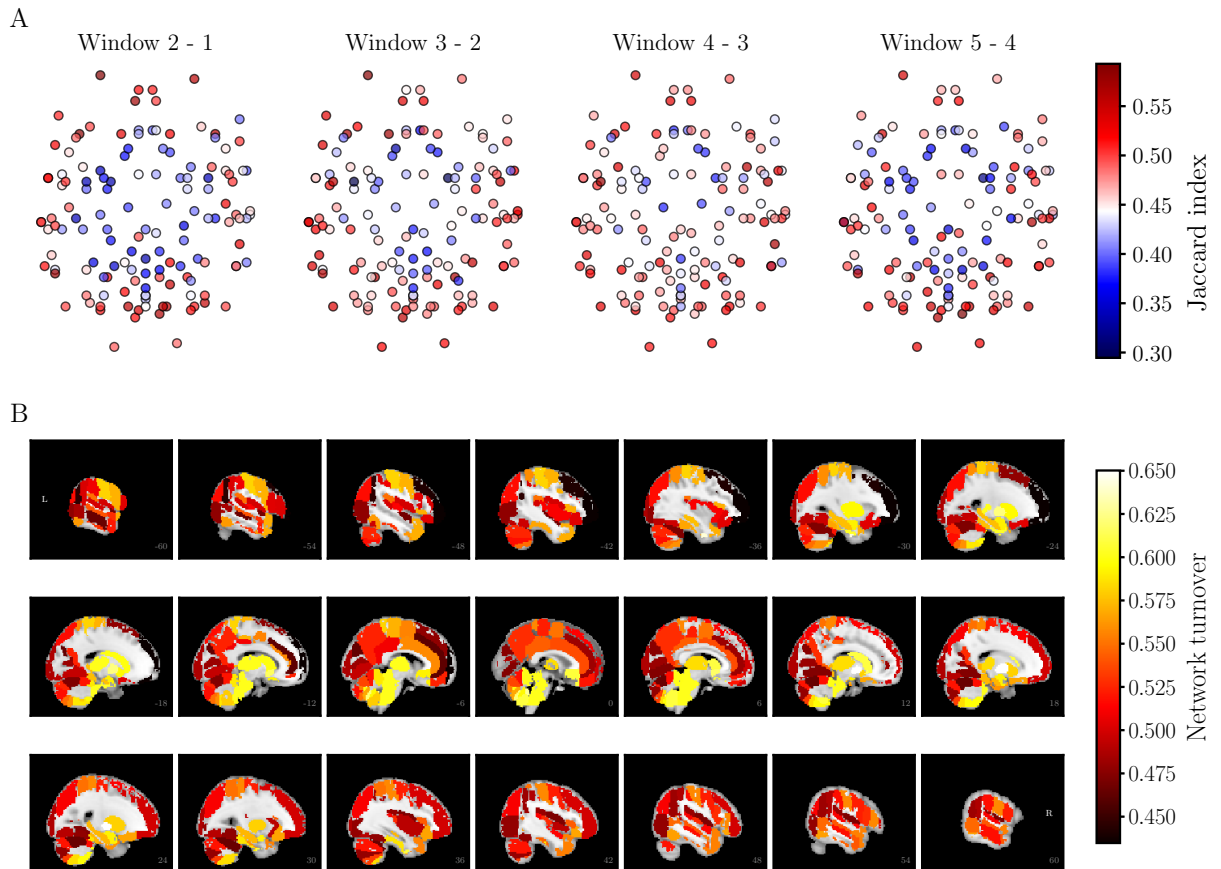


Figure S7: Changes in local network structure in the HO atlas. A) The Jaccard index between subsequent time windows. B) Network turnover on brain surface. All results are averaged over 13 subjects. For further details, see Fig. S6 and Fig. 3 of the main article.

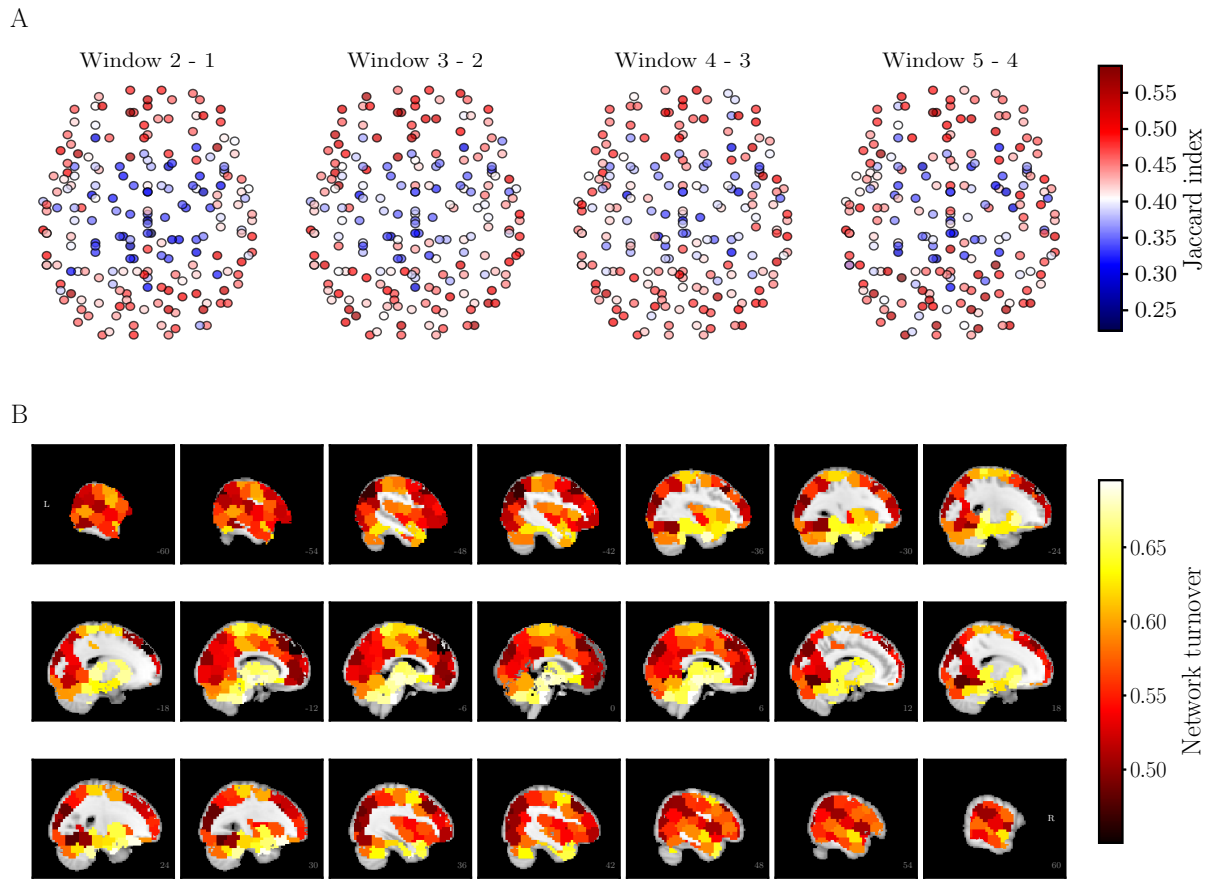


Figure S8: Changes in local network structure in the Craddock 200 atlas. A) The Jaccard index between subsequent time windows. B) Network turnover on brain surface. All results are averaged over 13 subjects. For further details, see Fig. S6 and Fig. 3 of the main article.

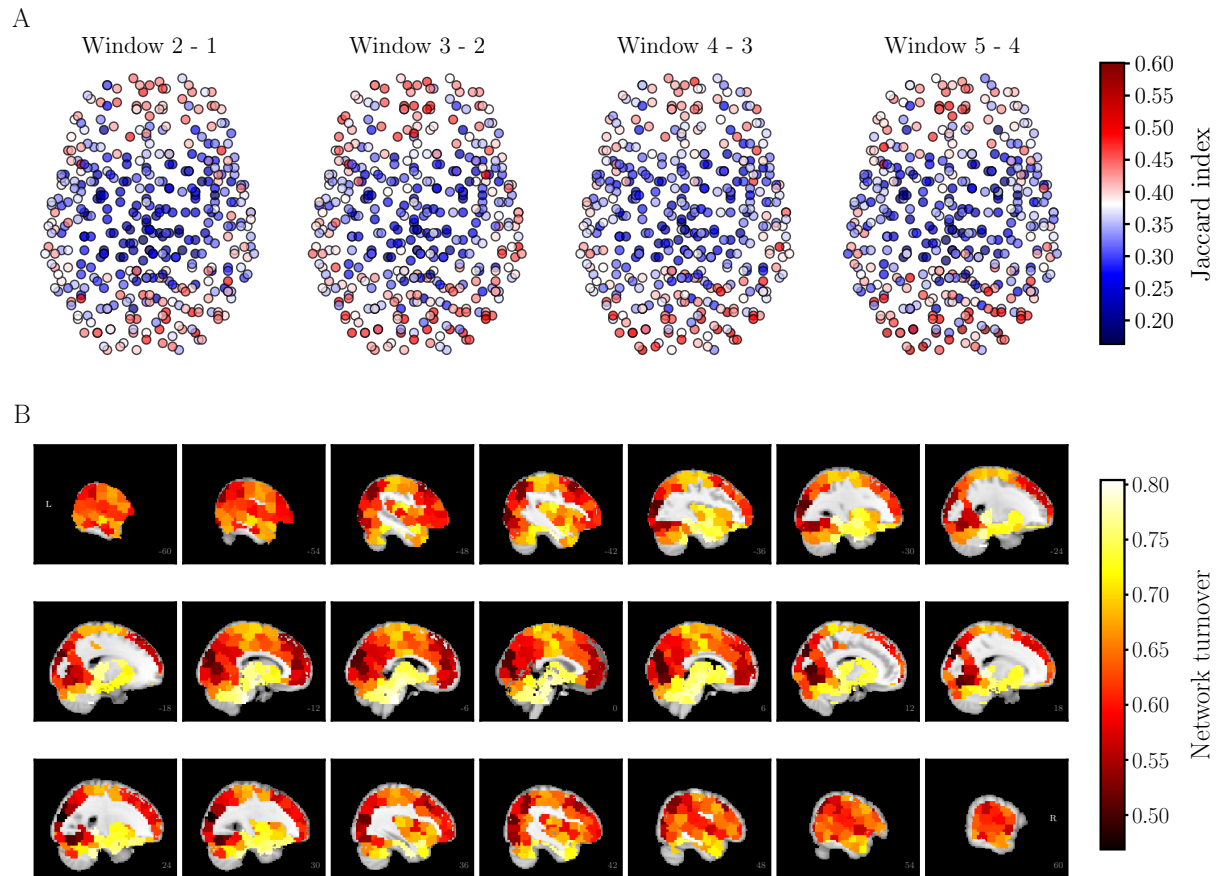


Figure S9: Changes in local network structure in the Craddock 400 atlas. A) The Jaccard index between subsequent time windows. B) Network turnover on brain surface. All results are averaged over 13 subjects. For further details, see Fig. S6 and Fig. 3 of the main article.

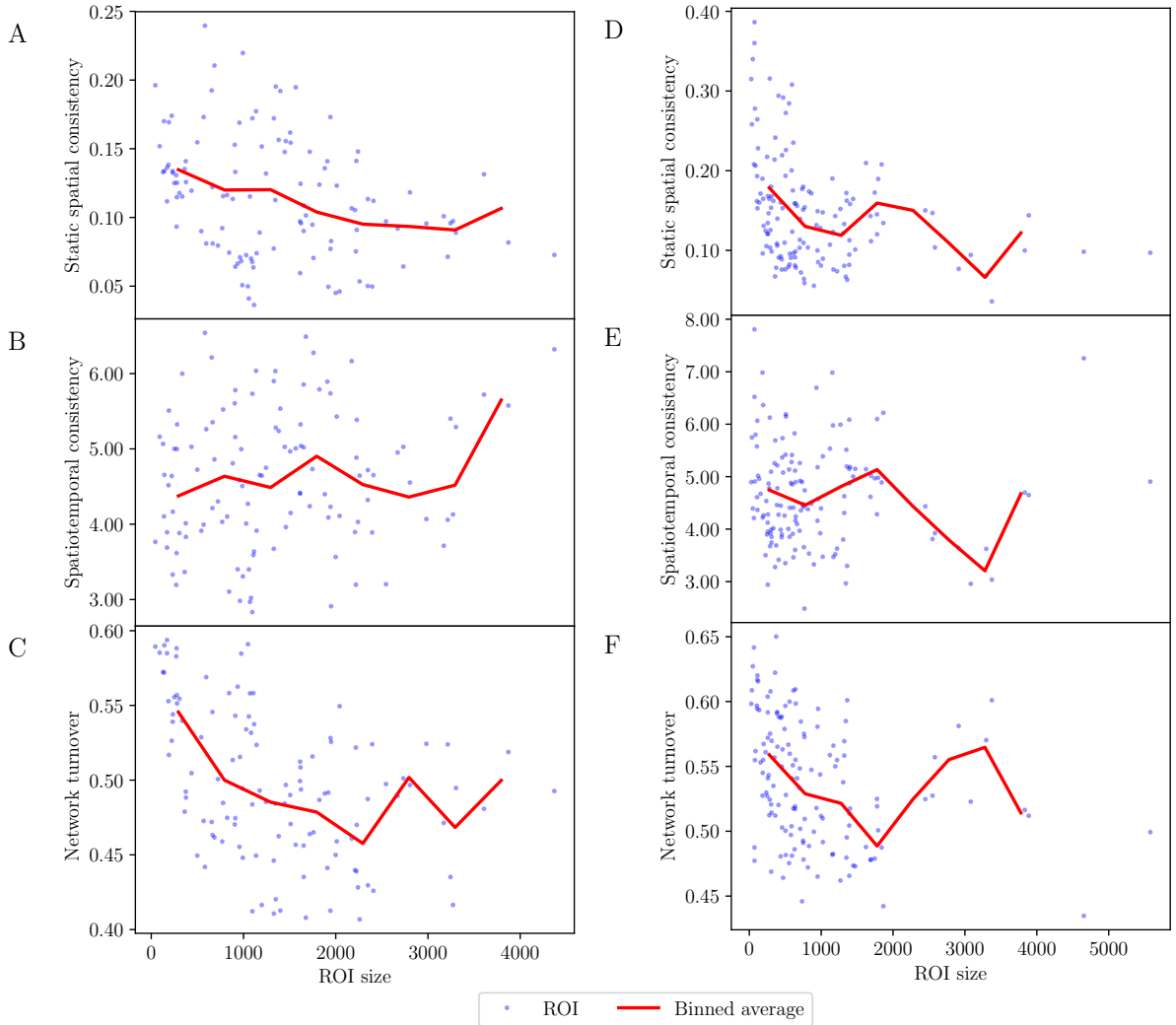


Figure S10: Relationship between sizes of AAL (left column) and HO (right column) ROIs and their spatial and spatiotemporal consistency and network turnover. There is a weak negative correlation between static spatial consistency and ROI size in both AAL (A) and HO (D). Spatiotemporal consistency does not correlate with ROI size either in AAL (B) or in HO (E). Network turnover is negatively correlated with ROI size in both AAL (C) and HO (F). All results are averages over 13 subjects. Solid red lines show bin averages, binning as in Fig. 4 of the main article.

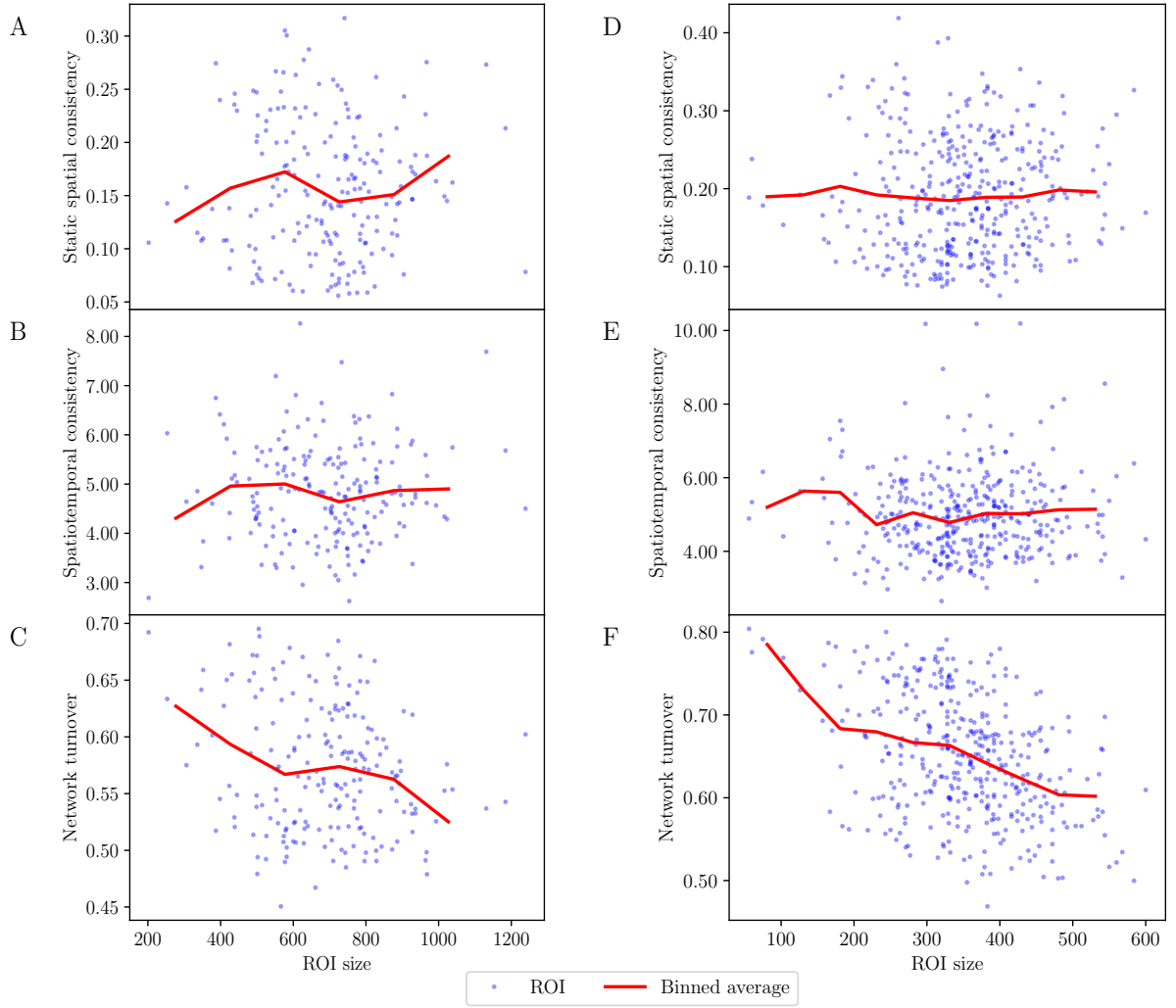


Figure S11: Relationship between sizes of Craddock 200 (left column) and Craddock 400 (right column) ROIs and their spatial and spatiotemporal consistency and network turnover. There is no correlation between static spatial consistency and ROI size in Craddock 200 (A) or Craddock 400 (D). Spatiotemporal consistency is not correlated with ROI size either in Craddock 200 (B) or in Craddock 400 (E). Network turnover correlates negatively with ROI size in both Craddock 200 (C) and Craddock 400 (F). All results are averages over 13 subjects. Solid red lines show bin averages, binning as in Fig. 4 of the main article.

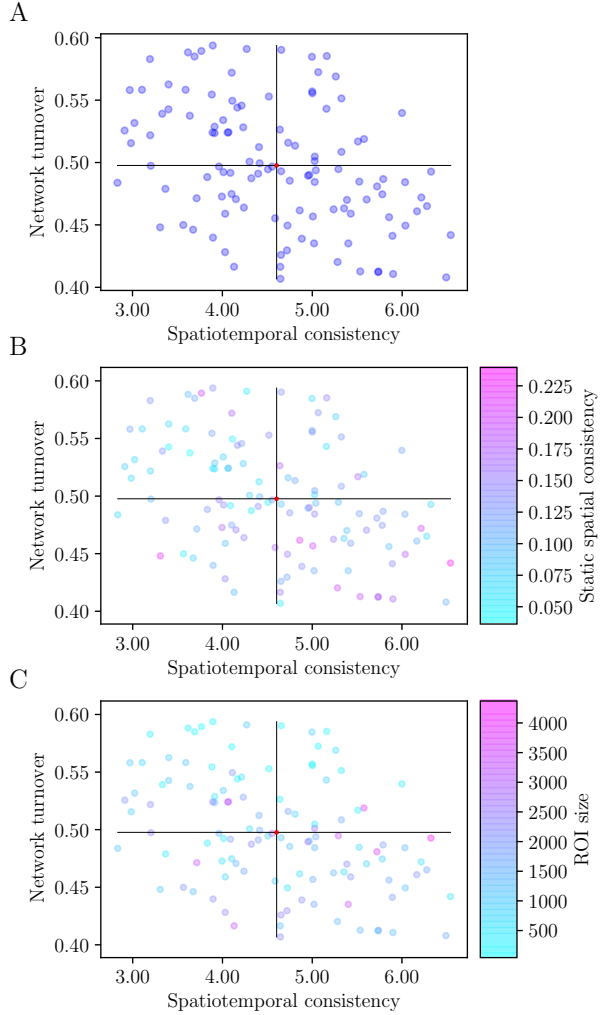


Figure S12: Relationship between static spatial consistency, spatiotemporal consistency, and network turnover in the AAL atlas. A) Spatiotemporal consistency is negatively correlated with network turnover, similarly as in the Brainnetome atlas (see Fig. 5 of the main article). B) ROIs with the highest static spatial consistency tend to have also the highest spatiotemporal consistency and the lowest network turnover. C) ROIs with high spatiotemporal consistency and low network turnover tend to be larger than ROIs with small spatiotemporal consistency and high network turnover. All results are averages over 13 subjects.

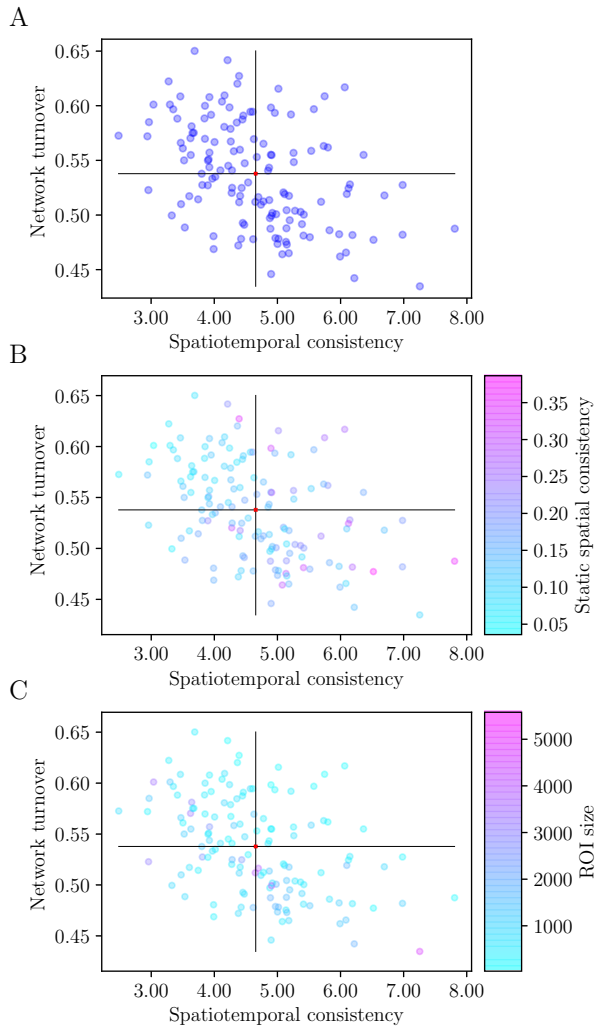


Figure S13: Relationship between static spatial consistency, spatiotemporal consistency, and network turnover in the HO atlas. A) Spatiotemporal consistency and network turnover are negatively correlated. B) ROIs with the highest static spatial consistency also have the highest spatiotemporal consistency and lowest network turnover. C) No clear connection is visible between ROI size, spatiotemporal consistency, and network turnover. All results are averages over 13 subjects.

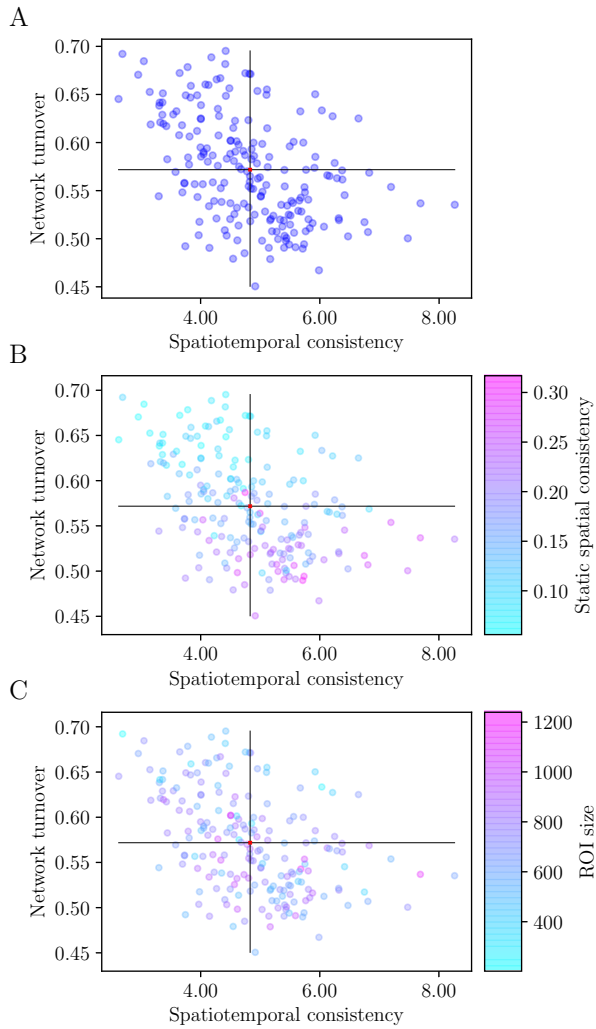


Figure S14: Relationship between static spatial consistency, spatiotemporal consistency, and network turnover in the Craddock 200 atlas. A) Spatiotemporal consistency correlates negatively with network turnover. B) ROIs with the highest static spatial consistency also have the highest spatiotemporal consistency and lowest network turnover. C) No clear connection is visible between ROI size, spatiotemporal consistency, and network turnover. All results are averages over 13 subjects.

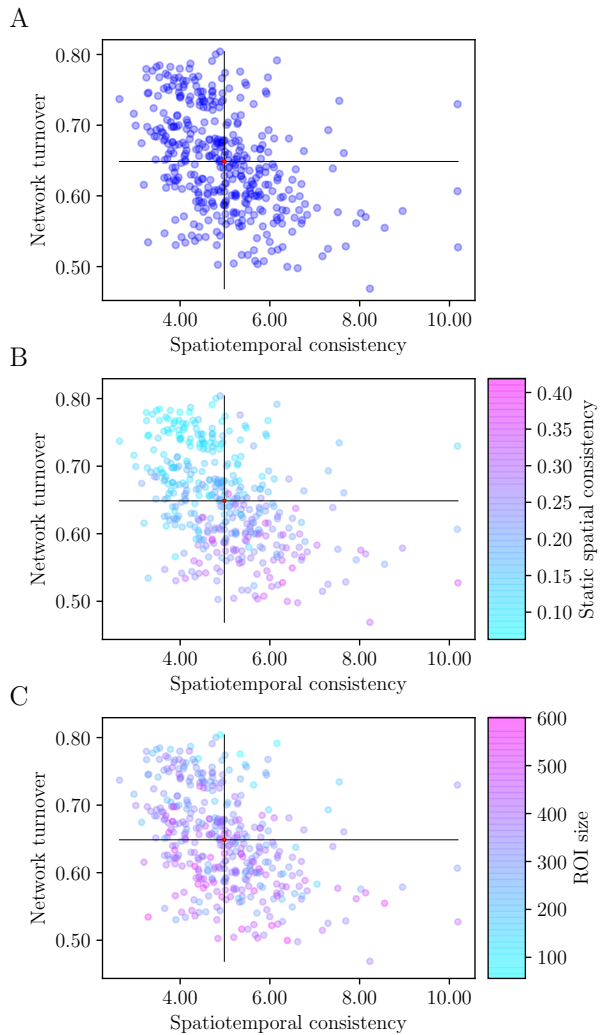


Figure S15: Relationship between static spatial consistency, spatiotemporal consistency, and network turnover in the Craddock 400 atlas. A) Spatiotemporal consistency correlates negatively with network turnover. B) ROIs with the highest static spatial consistency also have the highest spatiotemporal consistency and lowest network turnover. C) No clear connection is visible between ROI size, spatiotemporal consistency, and network turnover. All results are averages over 13 subjects.

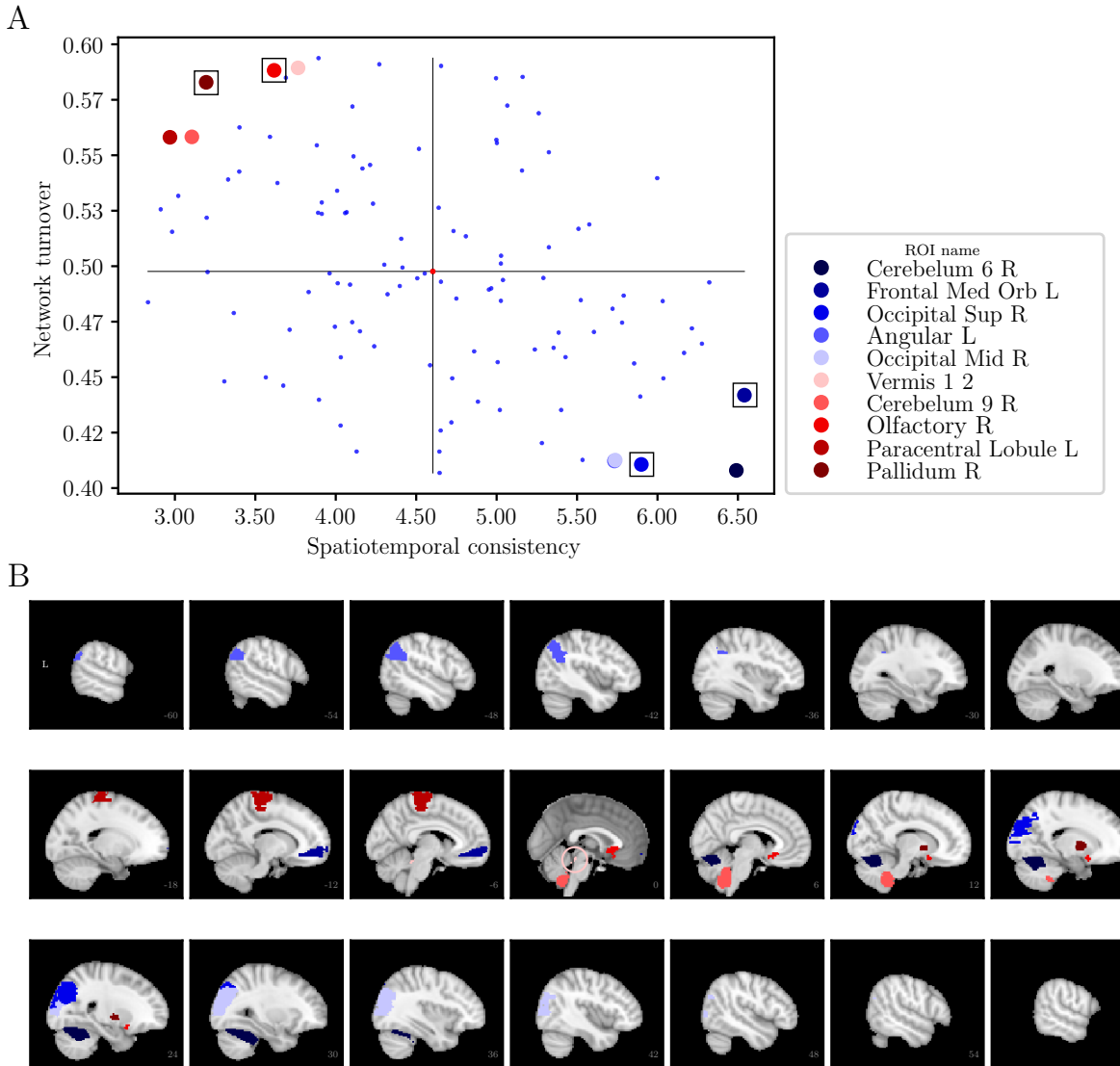


Figure S16: Extreme groups of ROIs in terms of spatiotemporal consistency and network turnover in the AAL atlas. A) Location of the extreme ROIs in the space spanned by spatiotemporal consistency and network turnover. Blue ROIs have high network turnover and low spatiotemporal consistency, whereas red ROIs have low network turnover and high spatiotemporal consistency. For further details, see the main article. For ROIs marked with a square, voxel-level intra-ROI correlation matrices are presented in Fig. S20. B) Anatomical location of the ROIs of the extreme groups. L: left, R: right, Med: medial, Orb: orbitofrontal, Sup: superior, Mid: middle.

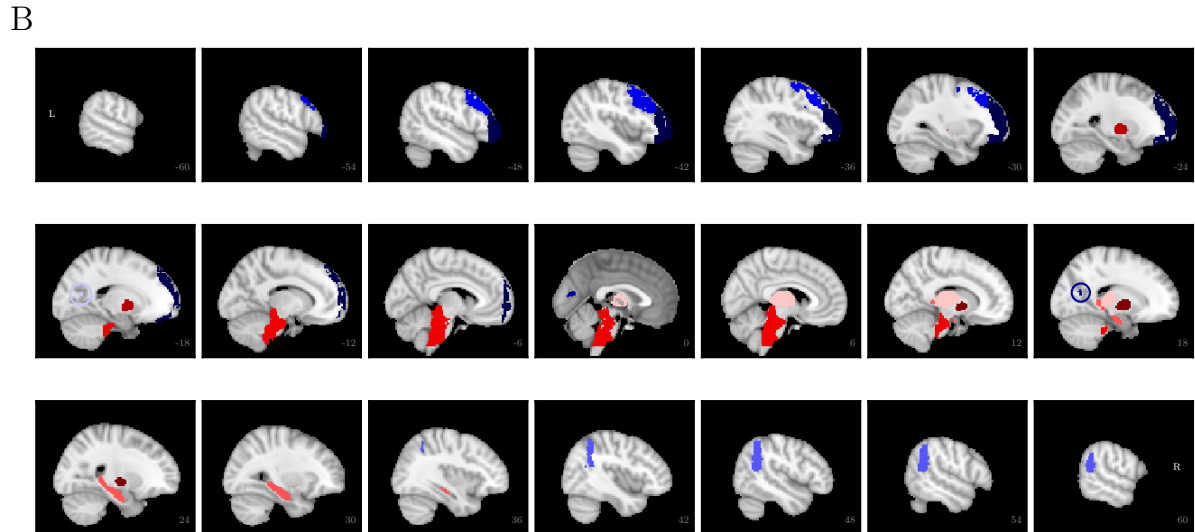
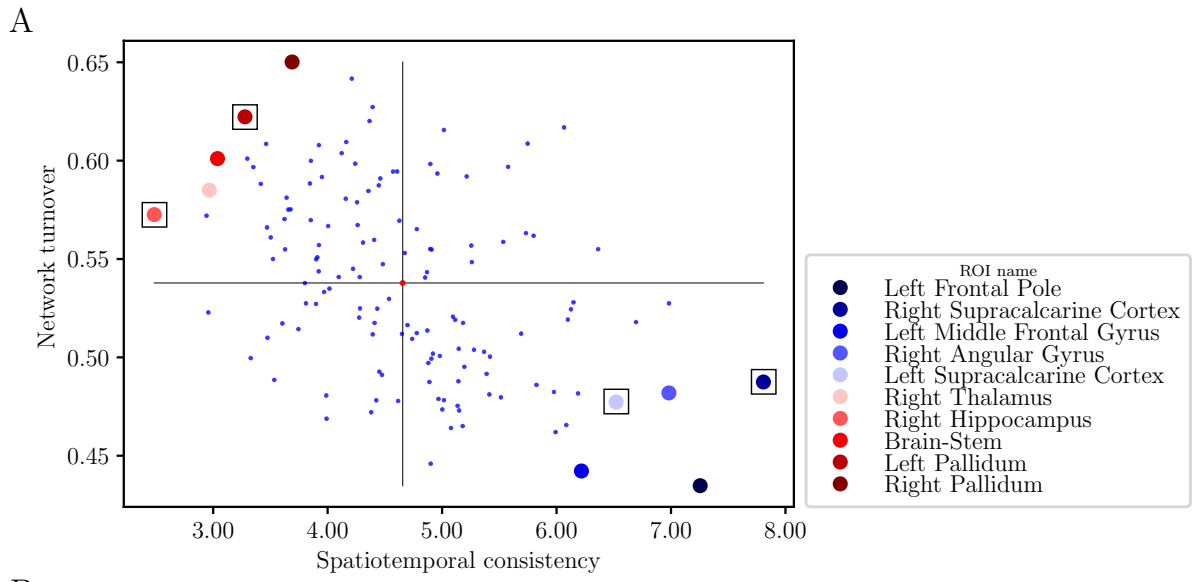
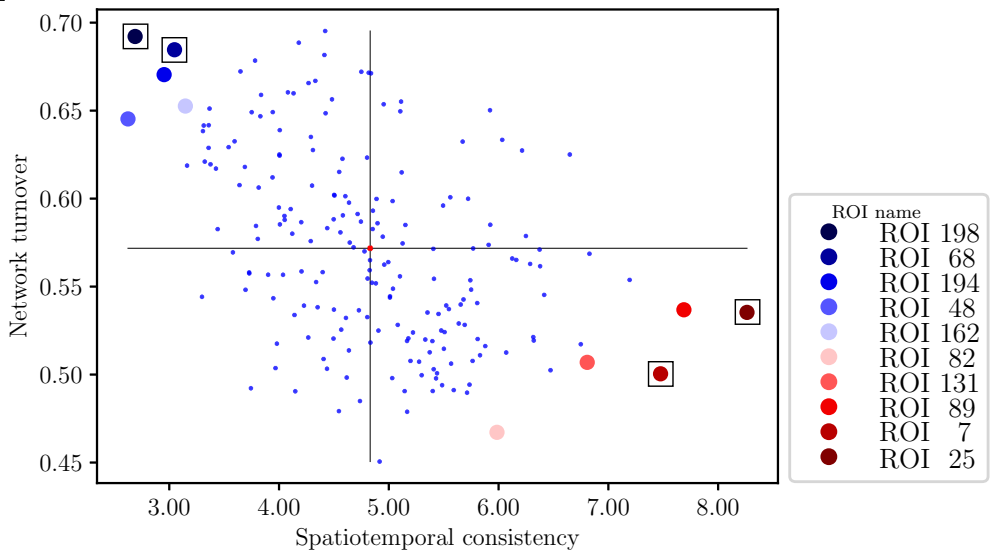


Figure S17: Extreme groups of ROIs in the HO atlas. A) Location of the extreme ROIs in the space spanned by spatiotemporal consistency and network turnover. For further details, see Fig. S16. B) Anatomical location of the extreme ROIs.

A



B

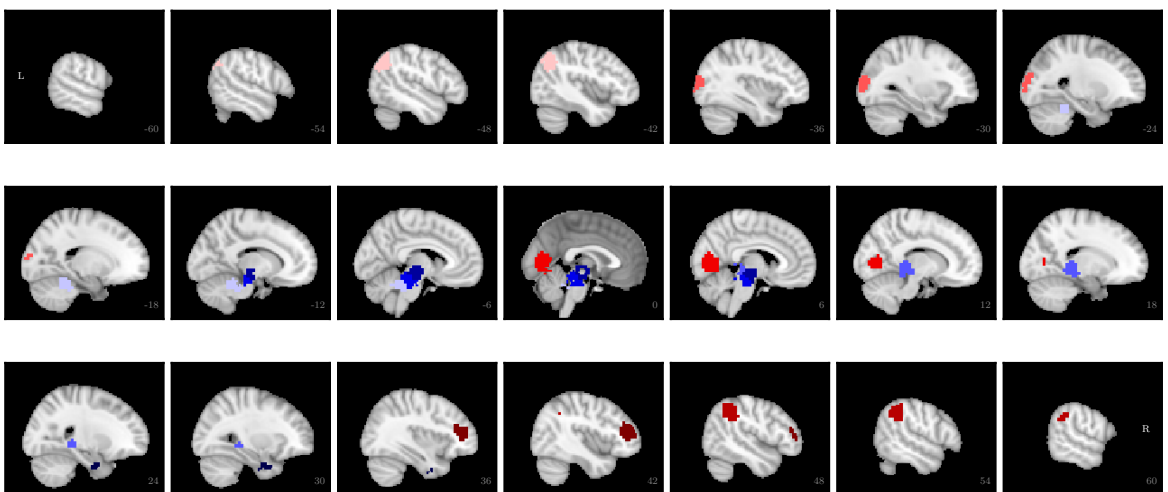


Figure S18: Extreme groups of ROIs in the Craddock 200 atlas. A) Location of the extreme ROIs in the space spanned by spatiotemporal consistency and network turnover. For further details, see Fig. S16. B) Anatomical location of the extreme ROIs.

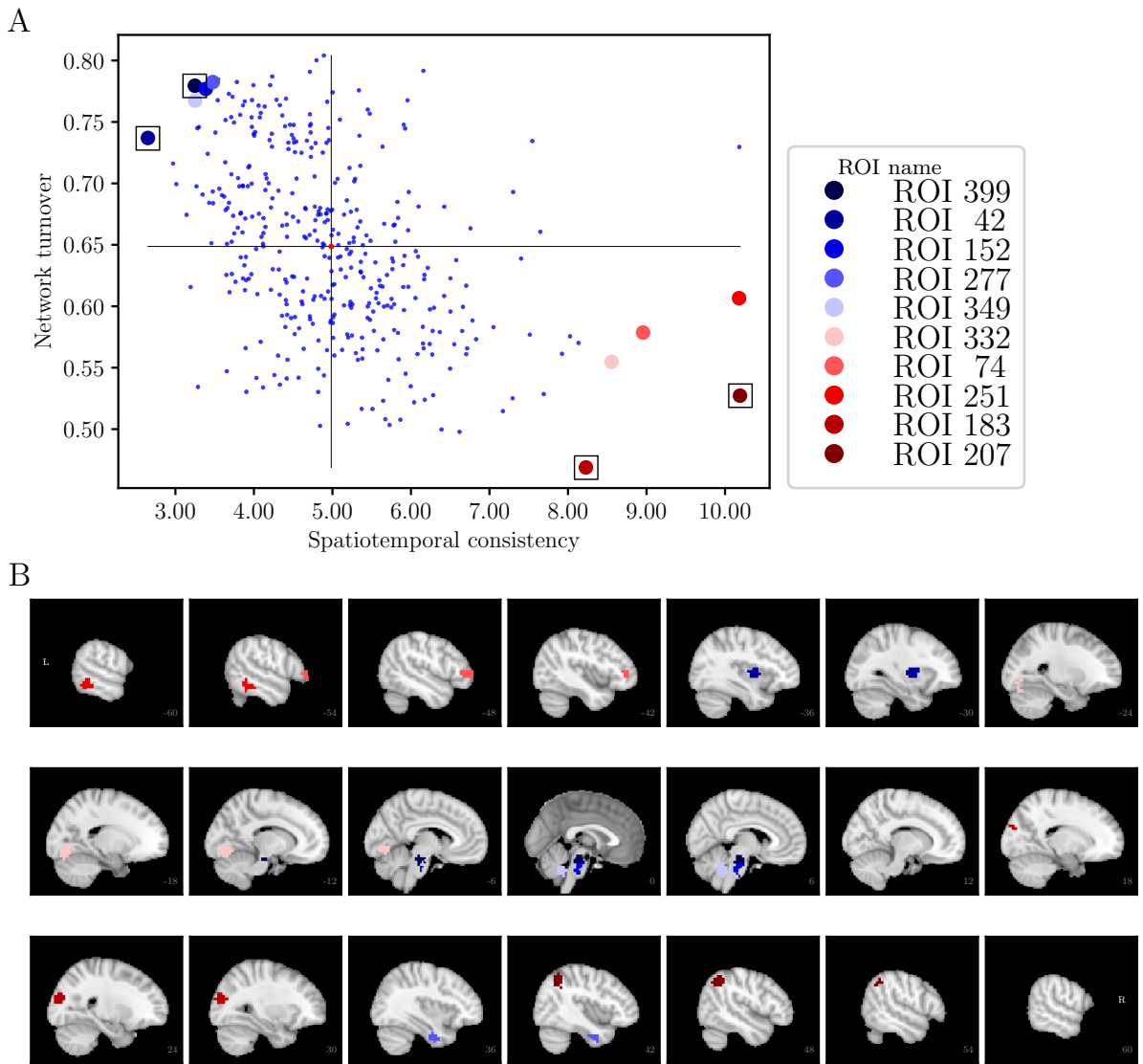


Figure S19: Extreme groups of ROIs in the Craddock 400 atlas. A) Location of the extreme ROIs in the space spanned by spatiotemporal consistency and network turnover. For further details, see Fig. S16. B) Anatomical location of the extreme ROIs.

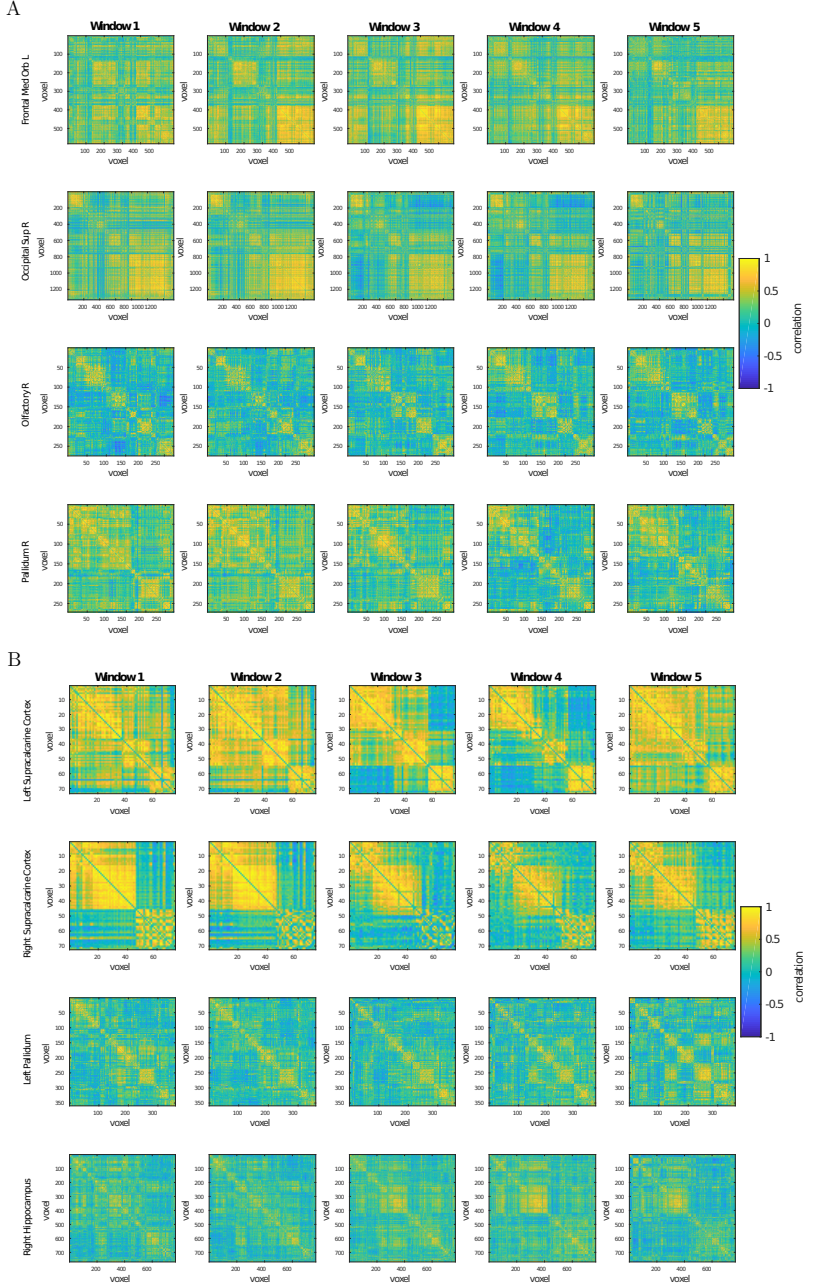


Figure S20: Internal connectivity of ROIs in AAL (A) and HO (B) atlases visualized in terms of intra-ROI voxel-level correlation matrices. For both atlases, the upper two rows display correlation matrices for ROIs with high spatiotemporal consistency and low network turnover (the red extreme group) and two lower rows matrices for ROIs with low spatiotemporal consistency and high network turnover (blue extreme group). For further details, see Fig. 7 of the main article.

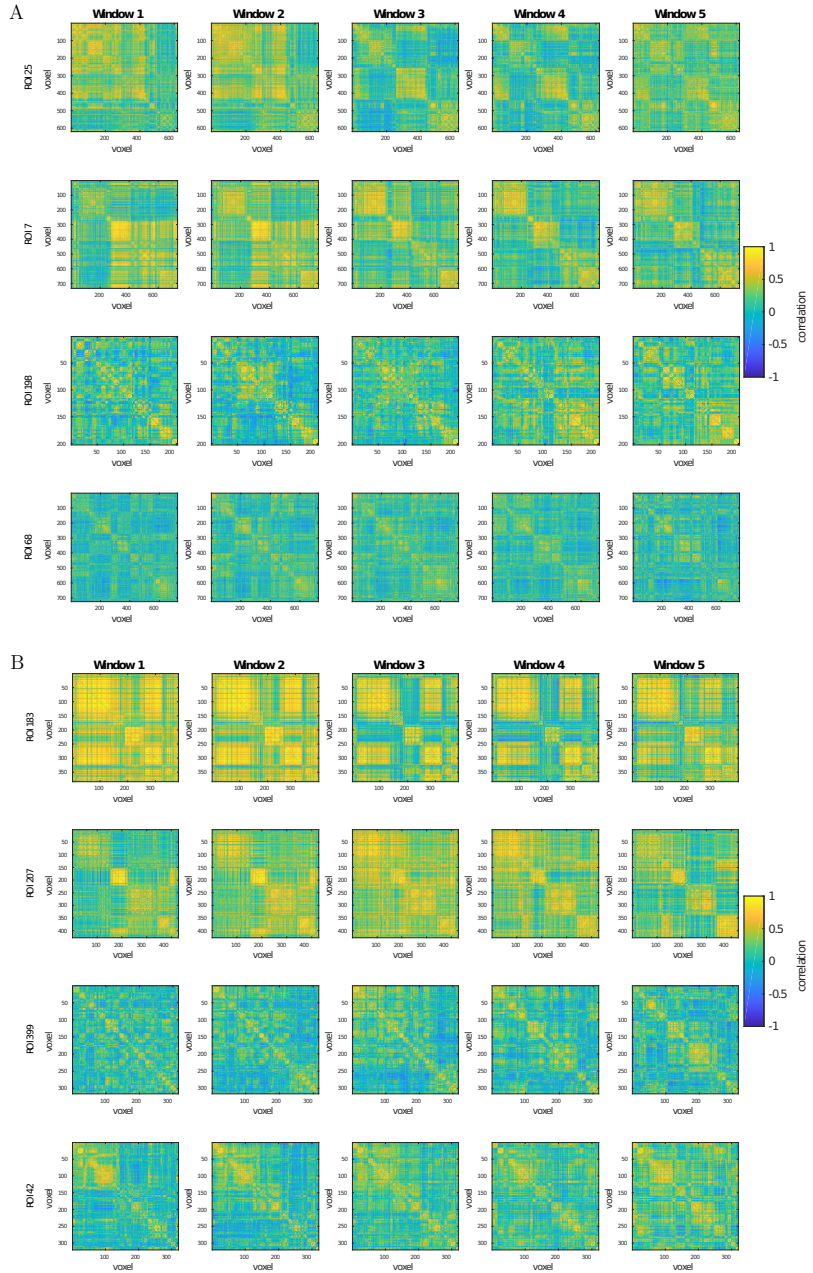


Figure S21: Internal connectivity of ROIs in Craddock 200 (A) and Craddock 400 (B) atlases visualized in terms of intra-ROI voxel-level correlation matrices. Similarly as in Fig. S20, the upper two rows display correlation matrices for ROIs with high spatiotemporal consistency and low network turnover (the red extreme group) and two lower rows matrices for ROIs with low spatiotemporal consistency and high network turnover (blue extreme group). For further details, see Fig. 7 of the main article.

2.2 ABIDE data

In order to ensure that the results are not explained by any specific feature of our in-house dataset, we repeated all analyses for a secondary, independent dataset, the ABIDE data. Results obtained using the ABIDE data were very similar to those obtained using the in-house data. Therefore, the results are reported here only briefly and the reader is referred to the main article for a more detailed discussion.

Although the maximum static spatial consistency is relatively high ($\phi_{spatial} = 0.761$), the distribution of static spatial consistency is broad and peaks at a low value ($\phi_{spatial} = 0.15$) (Fig. S22). There is a weak negative correlation between the size of a ROI and its static spatial consistency ($r = -0.21$, $p = 9.90 \times 10^{-4}$; Fig. S25A).

There is no visible difference between distributions of spatial consistency calculated in different time windows (Fig. S22). At the level of single ROIs, however, spatial consistency changes between subsequent time windows, the largest relative change being around 30% (Fig. S23A). These changes lead to an anatomically non-random distribution of spatiotemporal consistency (Fig. S23B), similarly as in the in-house data. The Brainnetome ROIs that have the highest mean spatiotemporal consistency are left precuneus (4_1), left thalamus (8_7 and 8_3), right cuneus (5_3), and right parahippocampal gyrus (6_4). ROIs with the lowest mean spatiotemporal consistency are left precentral gyrus (6_4), right postcentral gyrus (4_4), right striatum (6_1), right thalamus (8_2), and left parahippocampal gyrus (6_3). There is no significant correlation between ROI size and spatiotemporal consistency ($r = 0.039$, $p = 0.544$; Fig. S25B). There was a significant temporal correlation between spatial consistency and mean framewise displacement (FD) in one ROI, Amyg_L_2_1 (Pearson correlation coefficient $r = 0.54$, $p = 1.22 * 10^{-7}$, $FDR = 0.0152$). In other ROIs, there was no significant correlation between spatial consistency. Static spatial consistency and mean FD were not correlated for any of the ROIs.

Visible turnover takes place in the closest neighborhoods of nodes in the ABIDE data (Fig. S24A). Network turnover is anatomically nonuniformly distributed and shows strong spatial correlation (Fig. S24B). ROIs with the highest mean network turnover are right superior parietal lobule (5_3), left hippocampus (2_2), left precentral gyrus (6_3), left parahippocampal gyrus(6_5), and left inferior temporal gyrus (7_3). ROIs with the lowest mean network turnover include right cuneus (5_5), right precuneus (4_3), left superior occipital gyrus (2_1), left occipital gyrus (4_1), and right inferior parietal lobule (6_4). Similarly as in the in-house data, the ROIs with the highest network turnover are relatively small subcortical areas. There is a significant negative correlation ($r = -0.59$, $p \ll 10^{-5}$) between the size of a ROI and its network turnover (Fig. S25C).

Next, we investigated the relationship between spatiotemporal consistency and network turnover. In the ABIDE data, spatiotemporal consistency of ROIs varies between subjects more than in our in-house data. Because of this, the mean spatiotemporal consistency over subjects was, for some ROIs, exceptionally high. These outlier ROIs were clearly caused by very high values of spatiotemporal consistency in single subjects: when median over subjects was calculated instead of mean, no outlier ROIs were present. Therefore, we used

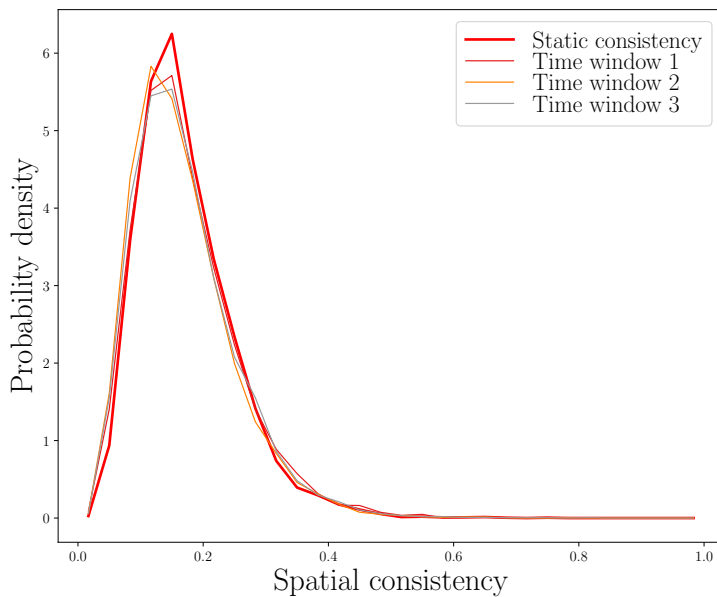


Figure S22: Functional homogeneity varies across ROIs in ABIDE data. Distribution of static spatial consistency (thick red line) and distributions of spatial consistency calculated separately in each of the three time windows of 80 samples. There is no visible difference between the distributions. In the ABIDE data, the time series are shorter than in the in-house data, which leads to a smaller number of time windows. All distributions have been calculated from pooled data of 28 subjects.

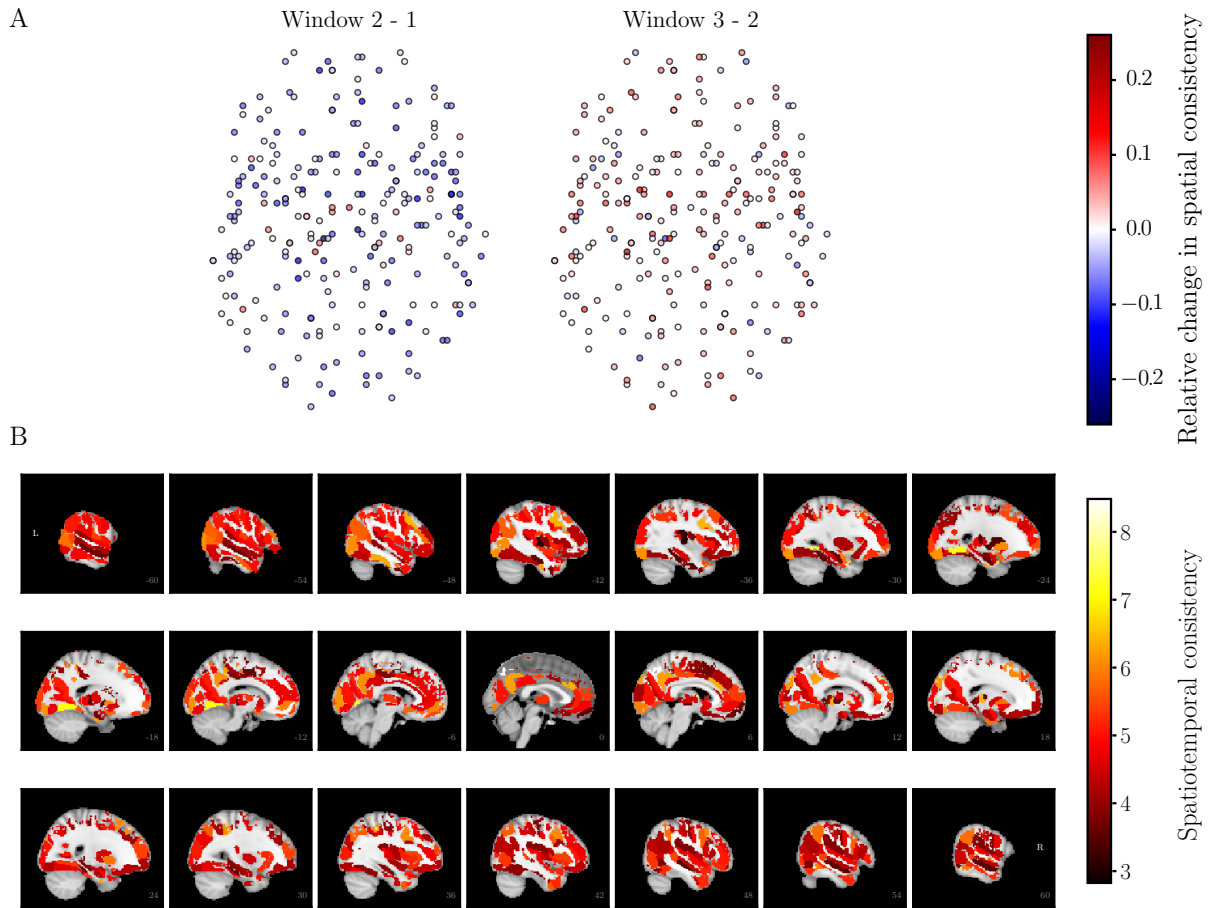


Figure S23: Spatial consistency of ROIs changes in time in ABIDE data. A) Relative changes in spatial consistency between subsequent time windows. Note that the ABIDE time series are shorter than the in-house time series, which leads to a smaller number of time windows. Changes are non-random in time, similarly as in the in-house data (see Fig. 2 of the main article). The location of the nodes is determined on the same way as in Fig. 2 of the main article. B) Spatiotemporal consistency on the brain surface. Spatiotemporal consistency is anatomically non-uniformly distributed and shows strong spatial correlation. All results are averages over 28 subjects. Grayscale areas are not included in the present study (white matter and cerebellum). Note that in the ABIDE data, ROIs are on average smaller than in the in-house data and there are more voxels that do not belong to same ROI for all subjects. In the visualization, these voxels are colored with grayscale.

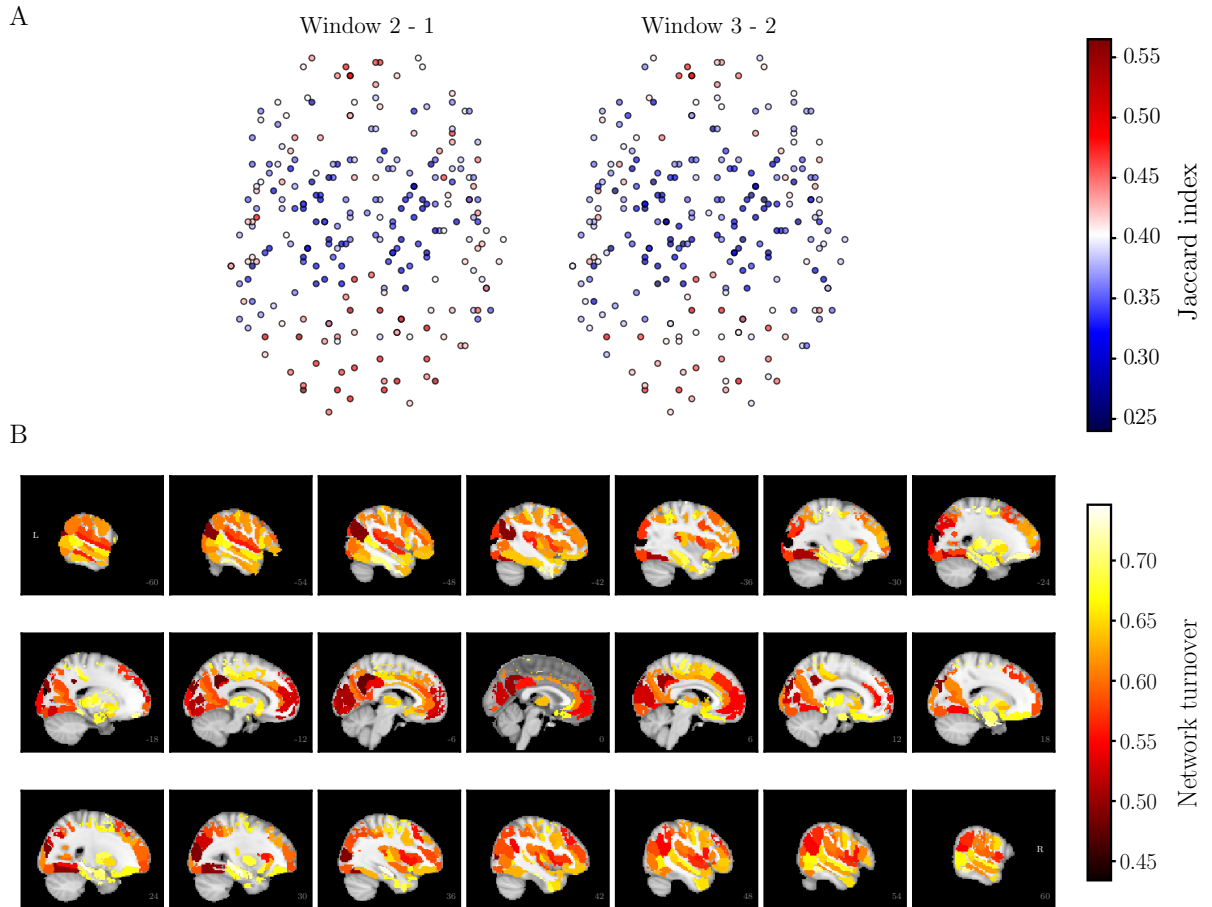


Figure S24: Significant neighborhood turnover takes place in the functional brain networks extracted from the ABIDE data. A) The Jaccard index between subsequent time windows. Values of the Jaccard index shows strong spatial correlation similarly as in the in-house data (see Fig. 3 of the main article). Node locations are defined as in Fig. 2 of the main article. B) Network turnover on the brain surface. High network turnover of subcortical areas is clearly visible. All results are averages over 28 subjects. For further details of the visualization, see Fig. S23.

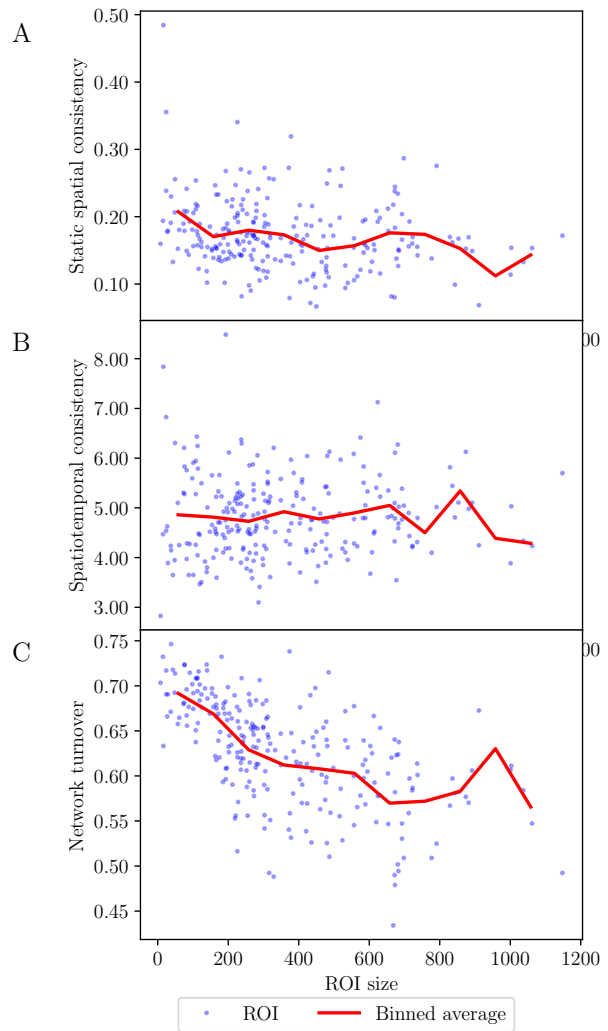


Figure S25: Relationship between the size of ROIs and their spatial and spatiotemporal consistency and network turnover in the ABIDE data. A) Static spatial consistency is negatively correlated with ROI size. B) There is no significant correlation between ROI size and spatiotemporal consistency. C) Network turnover is negatively correlated with ROI size. All results are averages over 28 subjects. The solid red lines show bin averages, binning as in Fig. 4 of the main article.

median instead of mean in the analysis of the ABIDE data.

Spatiotemporal consistency and network turnover are negatively correlated at the group level ($r = -0.20$, $p = 1.92 \times 10^{-3}$; Fig. S26A). ROIs with the highest static spatial consistency tend to have also high spatiotemporal consistency and low network turnover, similarly as in the in-house data (Fig. S26B). These ROIs also tend to be larger than ROIs with low spatiotemporal consistency and high network turnover (Fig. S26C).

At the level of single subjects, the connection between spatiotemporal consistency and network turnover is less visible but still significant for some subjects (significant ($p < 0.05$) negative correlation for 7 subjects, negative but non-significant correlation for 13 subjects, and weak and non-significant positive correlation for 8 subjects).

With the help of PCA, we identified two groups of extreme ROIs: five ROIs with high spatiotemporal consistency and low network turnover and five ROIs with low spatiotemporal consistency and high network turnover (Fig. S27). In the ABIDE data, the first extreme group included left precuneus (4_1 and 4_4), right precuneus (4_3), left superior occipital gyrus (2_1), and right cuneus (5_3). The second extreme group contained left precentral gyrus (6_4), right striatum (6_1), left hippocampus (2_2), left inferior temporal gyrus (7_3), and right inferior temporal gyrus (7_1).

Finally, we selected four ROIs for a detailed investigation of internal connectivity. These ROIs were right precuneus (4_3), left superior occipital gyrus (2_1), left inferior temporal gyrus (7_3), and left hippocampus (2_2). The voxel-level correlation matrices of these ROIs reveal a rich internal connectivity structure (Fig. S28). Although the low-spatiotemporal-consistency ROIs and high-spatiotemporal-consistency ROIs differ from each other in terms of the overall voxel-level correlation, the internal structure is similar in all ROIs: voxels form several anticorrelated subareas. In all ROIs, this internal structure changes in time.

2.3 Spatial and spatiotemporal consistency obtained with the 1 TR shift sliding window approach

Dynamic functional connectivity is often studied using the 1 TR shift sliding window approach, where consecutive time windows are separated from each other by only one time frame (Keilholz, Caballero-Gaudes, Bandettini, Deco, & Calhoun, 2017). Therefore, the overlap between consecutive windows is maximal: $1 - l_{window}$. This approach is not entirely suitable for the present study: when the overlap between consecutive time windows gets too large, the changes in local network structure are not visible anymore. Indeed, the mean Jaccard index between ROIs' closest neighborhoods in 5 consecutive 1 TR shift windows got a value as high as 0.9252 (average over subjects, ROIs, and window pairs), indicating that no changes in the local network structure could be obtained with this approach.

However, we investigated if time-dependent changes in spatial consistency could be obtained using this common approach. To this end, we used the Brainnetome parcellation. Less surprisingly, there were no visible differences between the distributions of spatial consistency obtained in consecutive time windows with the 1 TR shift approach (Fig. S29A). These distributions were also very close to those obtained using the 50%

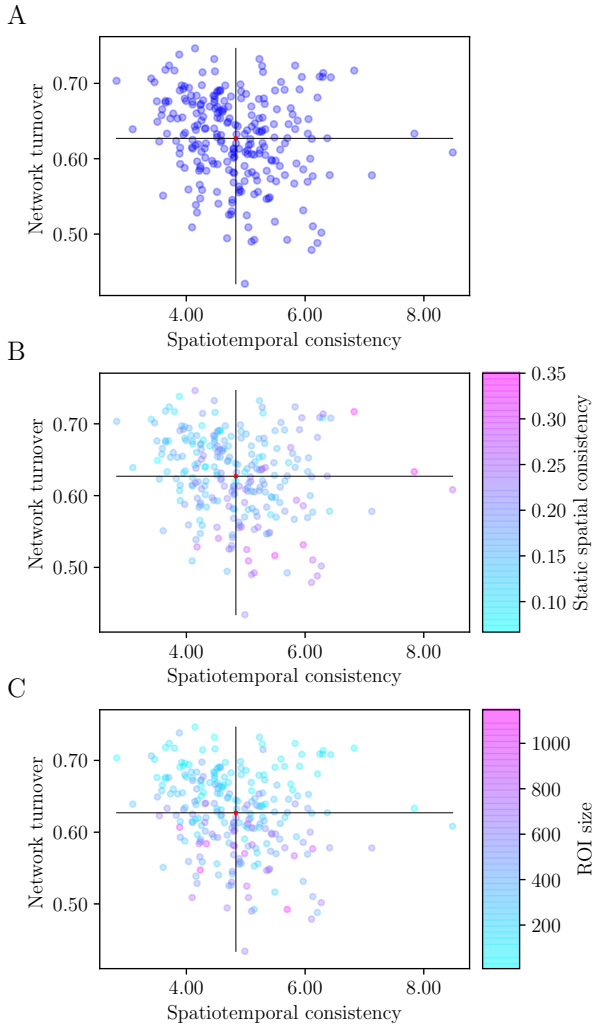
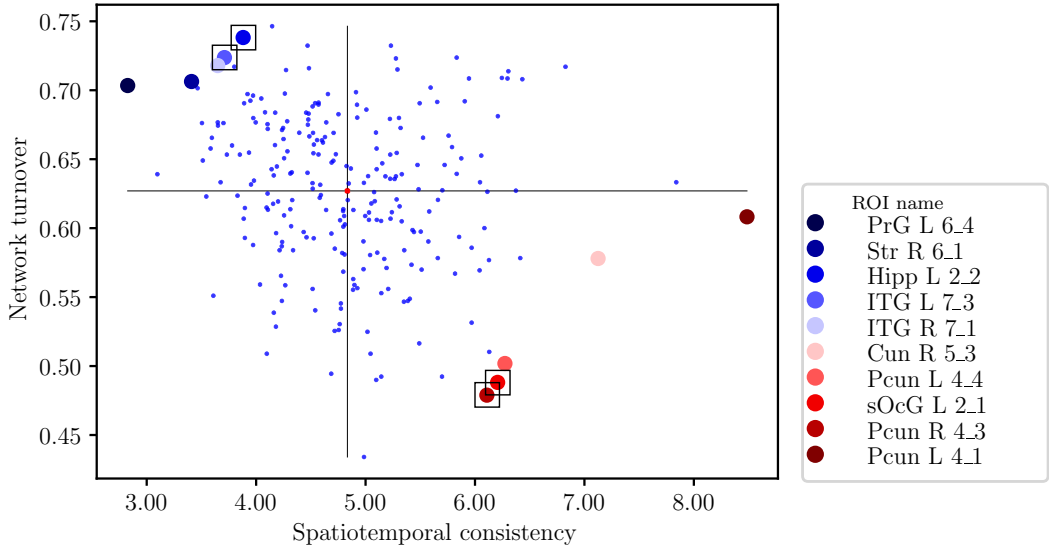


Figure S26: Relationship between static spatial consistency, spatiotemporal consistency, and network turnover in the ABIDE data. A) Spatiotemporal consistency and network turnover are negatively correlated. B) ROIs with the highest static spatial consistency tend to have also high spatiotemporal consistency and low network turnover. C) ROIs with high spatiotemporal consistency and low network turnover tend to be larger than ROIs with low spatiotemporal consistency or high network turnover. Note that unlike in Fig. 5 of the main article, here the median of spatiotemporal and network turnover over 28 subjects is visualized instead of average. For details, see the text.

A



B

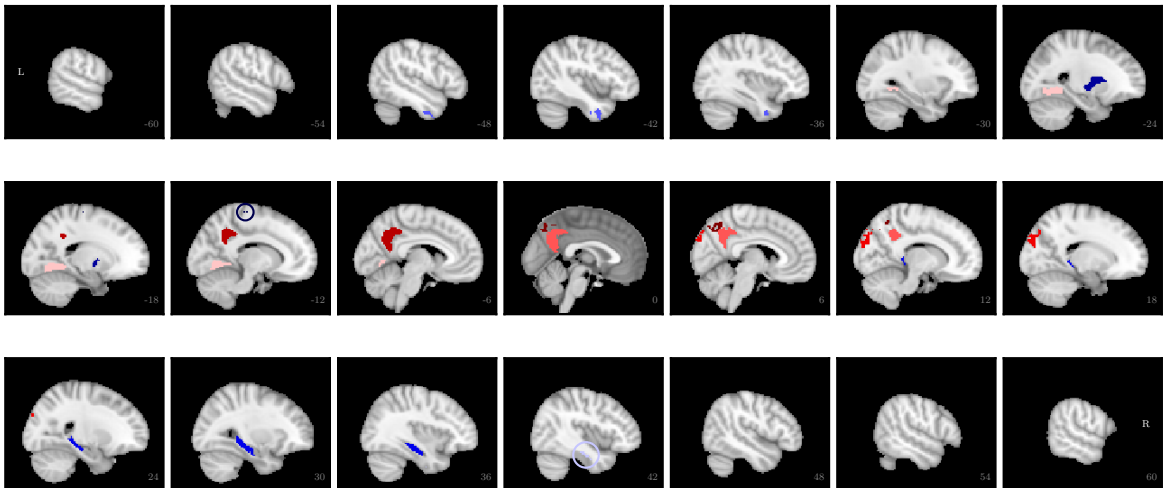


Figure S27: Extreme ROIs in terms of spatiotemporal consistency and network turnover in the ABIDE data. A) Location of extreme ROIs in the space spanned by spatiotemporal consistency and network turnover. Red ROIs have high spatiotemporal consistency and low network turnover, whereas blue ROIs have low spatiotemporal consistency and high network turnover. For further details, see Fig. 6 of the main article. B) Anatomical location of the extreme ROIs. L: left, R: right, PrG: precentral gyrus, Str: striatum, Hipp: hippocampus, ITG: inferior temporal gyrus, Cun: cuneus, Pcun: precuneus, sOcG: superior occipital gyrus

overlap windows (see Fig. 1B). Distribution of spatiotemporal consistency was slightly shifted to the right when the 1 TR shift approach was used (distribution peaks at $\phi_{st} = 3.1$ for 50% overlap vs $\phi_{st} = 4.9$ for 1 TR shift; Fig. S29B). This should not be surprising: as majority of the data used for calculating the spatial consistencies is shared between consecutive time windows, there is less space for variation between the time windows. However, the overall shape of the distributions was same with both the 50% overlap windows and the 1 TR shift approach, and low spatiotemporal consistencies that indicate significant relative changes in spatial consistency are present also when the 1 TR shift approach is used.

2.4 Connection between spatial consistency and time-resolved functional connectivity

Functional connectivity of the brain has been reported to fluctuate over time (Cocchi et al., 2017; Zalesky, Fornito, Cocchi, Gollo, & Breakspear, 2014), and these fluctuations have been suggested to underlie changes in cognitive processing (Cocchi et al., 2017). In order to investigate if the temporal variation of spatial consistency is related to these fluctuations, we obtained time-resolved functional connectivity as the mean weight of the 100 links whose weight changes the most in time (Cocchi et al., 2017; Zalesky et al., 2014). Further, we calculated for each time window the global efficiency that measures how well the network is connected. Then, we concatenated the values of time-resolved functional connectivity and global efficiency across subjects and calculated, for each ROI, the Pearson correlation coefficient between these values and the spatial consistency. All measures were obtained using 1 TR shift sliding windows, and the global efficiency was obtained in a network thresholded to $d = 20\%$ similarly as in (Cocchi et al., 2017). In Brainnetome, we obtained a significant correlation between spatial consistency and time-resolved functional connectivity for 11 ROIs (Pearson correlation coefficients between $r_{min} = 0.45$ and $r_{max} = 0.62$, $p < 0.001$, $FDR < 0.05$). In HO, spatial consistency and time-resolved functional connectivity correlated for 21 ROIs ($r_{min} = 0.53$, $r_{max} = 0.76$, $p < 0.01$, $FDR < 0.05$). In AAL and Craddock 200/400, there were no significant correlations between spatial consistency and time-resolved functional connectivity. In all investigated parcellations, we observed a negative correlation between global efficiency and spatial consistency for some ROIs (Brainnetome: 16 ROIs, $r_{min} = -0.66$, $r_{max} = -0.42$, $p < 0.005$, $FDR < 0.05$; AAL: 18 ROIs, $r_{min} = -0.66$, $r_{max} = -0.38$, $p < 0.01$, $FDR < 0.05$; HO: 28 ROIs, $r_{min} = -0.67$, $r_{max} = -0.40$, $p < 0.01$, $FDR < 0.05$; Craddock 200: 13 ROIs, $r_{min} = -0.59$, $r_{max} = -0.41$, $p < 0.005$, $FDR < 0.05$; Craddock 400: 26 ROIs, $r_{min} = -0.70$, $r_{max} = -0.42$, $p < 0.005$, $FDR < 0.05$). In the ABIDE dataset, there was a significant positive correlation between time-resolved functional connectivity and spatial consistency for 34 ROIs (Pearson correlation coefficients between $c_{min} = 0.32$ and $c_{max} = 0.63$, $pp < 0.01$, $FDR < 0.05$). Global efficiency correlated negatively with spatial consistency for 45 ROIs ($c_{min} = -0.43$, $c_{max} = -0.27$, $pp < 0.01$, $FDR < 0.05$).

2.5 An alternative measure for spatiotemporal consistency

In the main article, we found a negative correlation between spatiotemporal and network turnover of a ROI. This correlation, however, strongly depends on how we define spatiotemporal consistency. The definition given in equation (3) of the main article measures stability in terms of relative change: the most stable ROIs are those that have, on average, the smallest relative change in spatial consistency. For a more complete picture, we also investigated an alternative measure of spatiotemporal consistency: the inverse of the standard deviation ($1/SD$). It quantifies stability in terms of the absolute deviation of spatial consistency from the mean over time windows. For this alternative measure, we obtained a *positive* correlation between network turnover and spatiotemporal consistency in Brainnetome ($r = 0.36$, $p \ll 10^{-5}$, Fig S30B) and no significant correlation in other parcellations (HO: $r = 0.14$, $p = 0.098$; AAL: $r = 0.11$, $p = 0.221$; Fig. S30D, F). Craddock 200: $r = 0.65$, $p \ll 10^{-5}$, Craddock 400: $r = 0.63$, $p \ll 10^{-5}$.

At the first glance, this difference in results may look quite strange – the two measures of spatiotemporal consistency give the opposite results for the same ROIs. However, this can be understood by realizing that one of the measures is relative and the other is absolute. A ROI may show large absolute but small relative changes in spatial consistency between time windows if its spatial consistency is high on average. Indeed, those ROIs that have the highest spatiotemporal consistency in terms of relative change also have the highest static spatial consistency (Fig. 5B of the main article, Figs. S12B, S13B), which strongly correlates with the mean spatial consistency over separate time windows (Brainnetome: $r = 0.998$, $p \ll 10^{-5}$; HO: $r = 0.999$, $p \ll 10^{-5}$; AAL: $r = 0.999$, $p \ll 10^{-5}$; Craddock 200: $r = 0.999$, $p \ll 10^{-5}$; Craddock 400: $r = 0.999$, $p \ll 10^{-5}$). So, in summary, in ROIs with high static spatial consistency the variation of spatial consistency is absolutely large but relatively small.

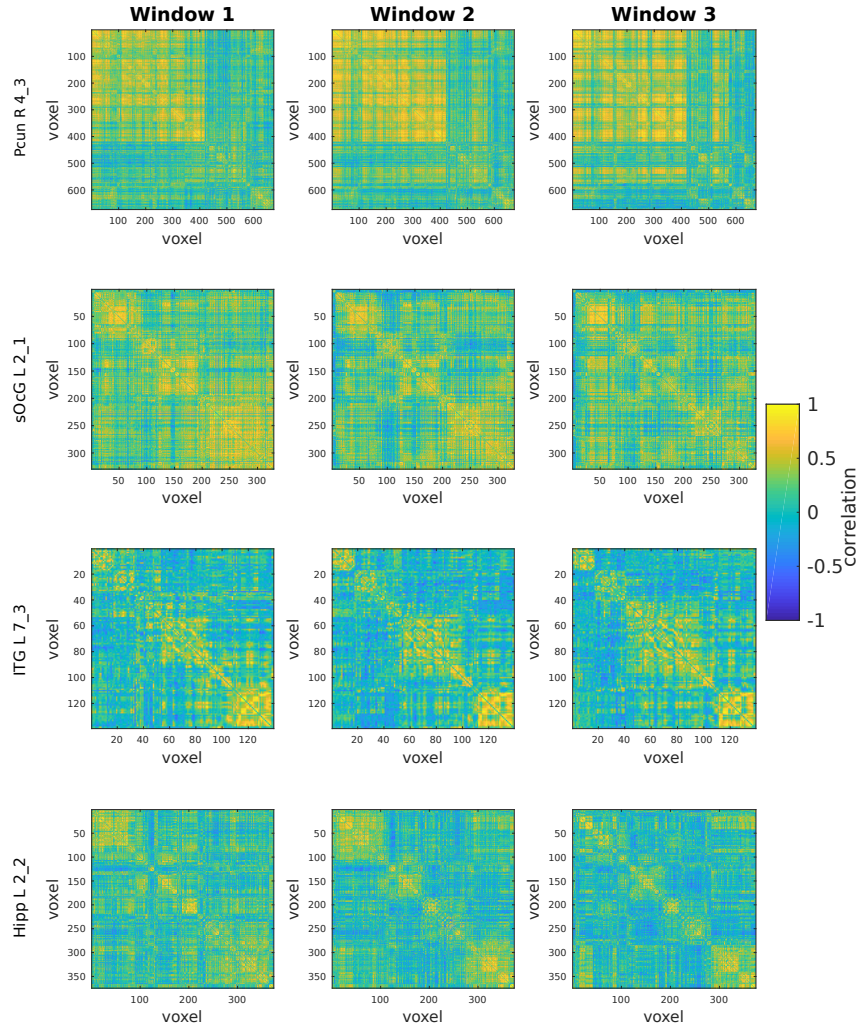


Figure S28: ROIs have rich internal connectivity structure in the ABIDE data, which is visualized by voxel-level intra-ROI correlation matrices. This structure changes in time. The upper two rows show matrices for ROIs with high spatiotemporal consistency and low network turnover, and the lower two ROIs show matrices for ROIs with low spatiotemporal consistency and high network turnover. For further details of visualization, see Fig. 7 of the main article. L: left, R: right, Pcun: precuneus, sOcG: superior occipital gyrus, ITG: inferior temporal gyrus, Hipp: hippocampus.

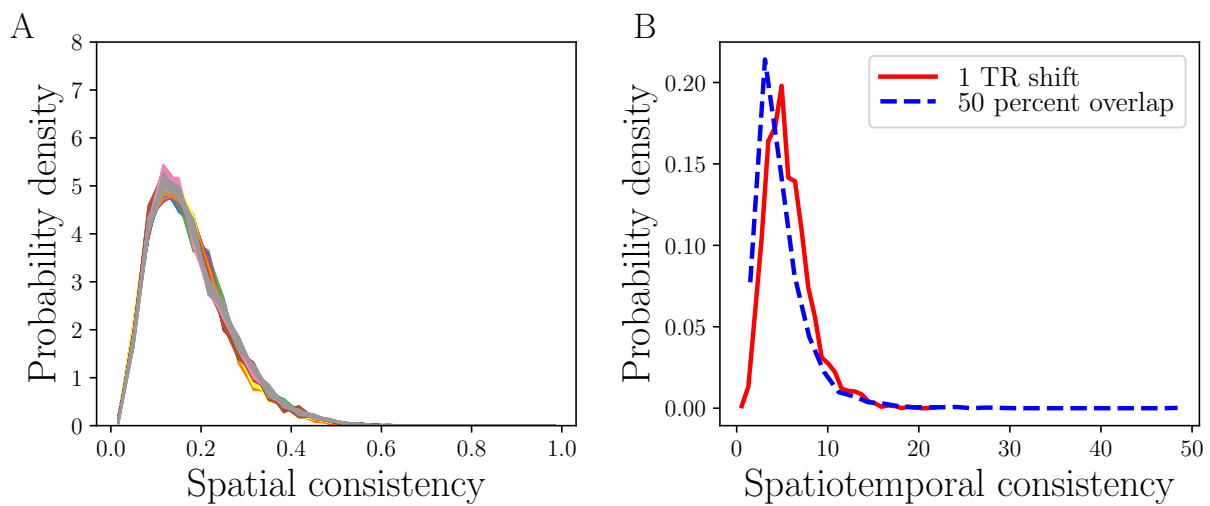


Figure S29: 1 TR shift approach does not affect the shape of spatial and spatiotemporal consistency distributions. A) Distributions of spatial consistency calculated separately in all the 165 time windows of the 1 TR shift approach for the Brainnetome atlas. B) Distributions of spatiotemporal consistency in the Brainnetome atlas calculated using the 1 TR shift approach (red solid line) and the 50% overlap windows (blue dashed line). The 50% overlap windows were used for obtaining the results presented in the main article.

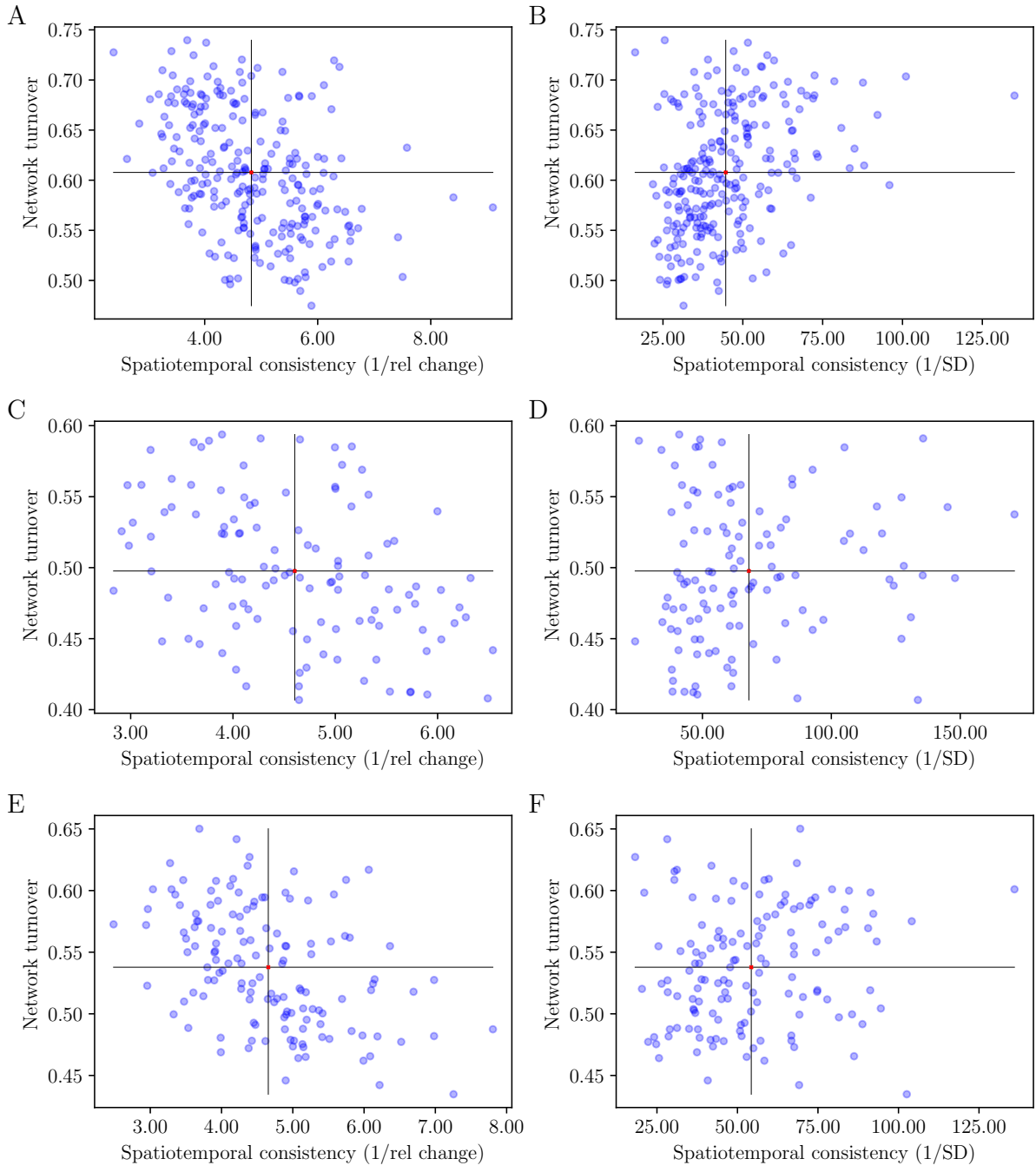


Figure S30: Definition of spatiotemporal consistency affects the relationship between spatiotemporal consistency and network turnover. When spatiotemporal consistency is defined in terms of relative change, spatiotemporal consistency and network turnover are negatively correlated in Brainnetome (A), AAL (C), and HO (E). However, an alternative definition of spatiotemporal consistency emphasizes absolute changes and leads to positive correlation in Brainnetome (B) and to no significant correlation in AAL (D) and HO (F). For discussion about differences in the two definitions of spatiotemporal consistency, see the text.

References

- Bassett, D. S., Wymbs, N. F., Porter, M. A., Mucha, P. J., Carlson, J. M., & Grafton, S. T. (2011). Dynamic reconfiguration of human brain networks during learning. *Proceedings of the National Academy of Sciences*, 108(18), 7641–7646. doi: 10.1073/pnas.1018985108
- Bassett, D. S., Wymbs, N. F., Rombach, M. P., Porter, M. A., Mucha, P. J., & Grafton, S. T. (2013). Task-based core-periphery organization of human brain dynamics. *PLoS Computational Biology*, 9(9), e1003171. doi: 10.1371/journal.pcbi.1003171
- Cocchi, L., Yang, Z., Zalesky, A., Stelzer, J., Hearne, L. J., Gollo, L. L., & Mattingley, J. B. (2017). Neural decoding of visual stimuli varies with fluctuations in global network efficiency. *Human Brain Mapping*, 38(6), 3069–3080. doi: 10.1002/hbm.23574
- Di Martino, A., Yan, C.-G., Li, Q., Denio, E., Castellanos, F. X., Alaerts, K., ... Milham, M. P. (2014). The autism brain imaging data exchange: towards a large-scale evaluation of the intrinsic brain architecture in autism. *Molecular psychiatry*, 19(6), 659–667. doi: 10.1038/mp.2013.78
- Keilholz, S., Caballero-Gaudes, C., Bandettini, P., Deco, G., & Calhoun, V. (2017). Time-resolved resting-state functional magnetic resonance imaging analysis: Current status, challenges, and new directions. *Brain connectivity*, 7(8), 465–481. doi: 10.1089/brain.2017.0543
- Leonardi, N., & Van De Ville, D. (2015). On spurious and real fluctuations of dynamic functional connectivity during rest. *Neuroimage*, 104, 430–436.
- Shakil, S., Billings, J. C., Keilholz, S. D., & Lee, C.-H. (2017). Parametric dependencies of sliding window correlation. *IEEE Transactions on Biomedical Engineering*. doi: 10.1109/TBME.2017.2762763
- Shakil, S., Keilholz, S. D., & Lee, C.-H. (2015). On frequency dependencies of sliding window correlation. In *2015 ieee international conference on bioinformatics and biomedicine (bibm)* (pp. 363–368). doi: 10.1109/BIBM.2015.7359708
- Zalesky, A., Fornito, A., Cocchi, L., Gollo, L. L., & Breakspear, M. (2014). Time-resolved resting-state brain networks. *Proceedings of the National Academy of Sciences*, 111(28), 10341–10346. doi: 10.1073/pnas.1400181111